APOE4 accelerates advanced-stage vascular and neurodegenerative disorder in old Alzheimer's mice via cyclophilin A independently of amyloid-β

Axel Montagne[1,4], **Angeliki M. Nikolakopoulou**[1,4], **Mikko T. Huuskonen**[1,4], **Abhay P. Sagare**[1,4], **Erica J. Lawson**[1], **Divna Lazic**[1], **Sanket V. Rege**[1], **Alexandra Grond**[1], **Edward Zuniga**[1], **Samuel R. Barnes**[2], **Jacob Prince**[1], **Meghana Sagare**[1], **Ching-Ju Hsu**[1], **Mary J. LaDu**[3], **Russell E. Jacobs**[1], **Berislav V. Zlokovic**[1,✉]

[1]Department of Physiology and Neuroscience, Zilkha Neurogenetic Institute, Keck School of Medicine, University of Southern California, Los Angeles, CA, USA.

[2]Department of Radiology, Loma Linda University, Loma Linda, CA, USA.

[3]Department of Anatomy and Cell Biology, College of Medicine, University of Illinois at Chicago, Chicago, IL, USA.

[4]These authors contributed equally: Axel Montagne, Angeliki M. Nikolakopoulou, Mikko T. Huuskonen, Abhay P. Sagare.

Abstract

Apolipoprotein E4 (*APOE4*), the main susceptibility gene for Alzheimer's disease (AD), leads to vascular dysfunction, amyloid-β pathology, neurodegeneration and dementia. How these different pathologies contribute to advanced-stage AD remains unclear. Using aged APOE knock-in mice crossed with *5xFAD* mice, we show that, compared to APOE3, APOE4 accelerates blood–brain barrier (BBB) breakdown, loss of cerebral blood flow, neuronal loss and behavioral deficits independently of amyloid-β. BBB breakdown was associated with activation of the

---

cyclophilin A-matrix metalloproteinase-9 BBB-degrading pathway in pericytes. Suppression of this pathway improved BBB integrity and prevented further neuronal loss and behavioral deficits in APOE4;5FAD mice while having no effect on amyloid-β pathology. Thus, APOE4 accelerates advanced-stage BBB breakdown and neurodegeneration in Alzheimer's mice via the cyclophilin A pathway in pericytes independently of amyloid-β, which has implication for the pathogenesis and treatment of vascular and neurodegenerative disorder in AD.

The *APOE4* variant of apolipoprotein E is the strongest genetic risk factor for AD[1]. One and two *APOE4* alleles increase risk for AD by approximately 4- and 15-fold, respectively, compared to the more-common *APOE3* gene that carries lower risk for AD[1]. Besides accelerating onset and progression of dementia, *APOE4* is associated with different brain pathologies. For example, *APOE4* accelerates BBB breakdown and degeneration of brain capillary pericytes[2,3] that maintain BBB integrity[4–6] and leads to cerebral blood flow (CBF) reduction[7,8] and dysregulation[7,9,10]. *APOE4* is toxic to neurons[11] and accelerates tau-mediated neurodegeneration[12]. Additionally, *APOE4* slows down amyloid-β (Aβ) clearance[13,14] and accelerates amyloid deposition14_16, which promotes development of amyloid pathology.

Recent studies focused on very early stages in the Alzheimer's continuum in individuals who are cognitively unimpaired or with mild cognitive impairment (MCI) have shown that individuals bearing an *APOE4* variant (*APOE3/APOE4* or *APOE4/APOE4*) are distinguished from *APOE3* homozygotes by breakdown in the BBB in the hippocampus and medial temporal lobe, regions responsible for memory encoding and cognitive functions[17]. This finding is apparent in cognitively unimpaired *APOE4* carriers and more severe in those with MCI and is independent of Aβ or tau pathology measured in the cerebrospinal fluid or in brain by positron emission tomography[17]. These findings support the growing evidence suggesting that vascular dysfunction, BBB breakdown and vascular disorder contribute to early cognitive impairment and AD[17–26]. On the other hand, accumulation of Aβ in the brain has also been suggested to occur years before cognitive impairment and continues to increase with disease progression[27]. Although it has been shown that vascular dysfunction contributes to early cognitive impairment in ways that may not be exclusively related to classical AD pathology[17,19,20,26], the respective contributions of the BBB pathway and vascular disorder versus amyloid-β pathway to advanced disease stage during progression of neurodegenerative disorder and cognitive decline in AD are still poorly understood.

To address this question, here we studied vascular dysfunction, Aβ pathology, neuronal dysfunction and behavior in older *APOE3* and *APOE4* knock-in mice[28] alone and crossed with the *5xFAD* line[29]. All mice were derived from the same litters, as previously described[30]. Mice lacking *Apoe*[3] and/or expressing human *APOE4* develop early BBB breakdown[3,31–33] and CBF dysregulation[10]. On the other hand, the *5xFAD* line also develops BBB breakdown[34–37], CBF reductions[38] and neuron and synaptic loss at a later stage[29,39], whereas *APOE3;5xFAD* and *APOE4;5xFAD* mice (also known as *E3FAD* and *E4FAD* lines, respectively[30]) have comparable Aβ pathology at an older age[40]. These features of the studied models allowed us to interrogate how different pathologies in *APOE4*

compared to *APOE3* mice relate to each other and how they influence neuronal function and behavior.

Results

Blood–brain barrier breakdown in *APOE4* and *APOE4;5xFAD* mice.

First, we studied BBB integrity in the cortex and hippocampus in 18–24-month-old *APOE3* and *APOE4* knock-in controls and *APOE3;5xFAD* and *APOE4;5xFAD* mice derived from the same litters, as previously described[30]. Using a dynamic contrast-enhanced magnetic resonance imaging (DCE-MRI) protocol as we previously developed[6,41], we found that *APOE4* mice compared to the respective *APOE3* lines develop accelerated BBB breakdown in the cortex and hippocampus both without and with Aβ pathology (Fig. 1a–c), as shown by 43% and 52% and 29% and 34% increases in the BBB permeability K_{trans} values in *APOE4* versus *APOE3* mice alone and in these mice crossed with *5xFAD* mice, respectively (Fig. 1b,c). We also found substantial 35% and 36% and 22% and 20% increases in regional BBB K_{trans} values in the cortex and hippocampus of *APOE3;5xFAD* and *APOE4;5xFAD* mice compared to their respective *APOE3* and *APOE4* littermate controls (Fig. 1c), consistent with previously shown BBB breakdown in *5xFAD* mice[34–37].

These results were confirmed by increased levels of perivascular brain capillary cortical and hippocampal deposits of blood-derived fibrinogen in *APOE4* compared to *APOE3* mice both in the presence and absence of Aβ pathology (Fig. 1d,e). Specifically, we found 111% and 122% and 135% and 137% increase in fibrinogen deposits in the cortex and hippocampus in *APOE4* versus *APOE3* mice alone and in these mice crossed with *5xFAD* mice, respectively (Fig. 1e). The effects of Aβ pathology was evident in both genotypes when compared to knock-in littermate controls (Fig. 1d,e), consistent with previously reported BBB breakdown in *5xFAD* mice.

In contrast to a previous study showing that younger 8-month-old *APOE4;5xFAD* female mice had higher BBB leakiness compared to male mice[42], the present study did not find the effect of gender on the regional BBB K_{trans} values in either *APOE4* versus *APOE3* mice alone and/or in these mice crossed with *5xFAD* mice (Extended Data Fig. 1). Whether the difference between previous studies[42] and the current study reflects a difference in age (18–24 versus 8 months old) and/or whether female mice develop less severe BBB impairment with age or alternatively, males develop more rapid BBB changes with age, remains an interesting topic for future studies.

Compared to *APOE3* mice, *APOE4* littermate controls showed loss of brain capillary pericyte coverage in the cortex and hippocampus (Fig. 1f,g). For example, *APOE4* compared to *APOE3* mice alone and crossed with *5xFAD* mice had 24% and 25% and 19% and 27% loss of pericyte coverage in the cortex and hippocampus, respectively (Fig. 1g). These findings were consistent with previously shown loss of pericyte coverage in *APOE4* mice[3]. The effect of Aβ pathology on loss of pericyte coverage was seen in both genotypes, again consistent with findings showing loss of pericytes in AD mouse lines[43–45]. However, the effect was much more pronounced in *APOE4* than in *APOE3* mice. The regional accumulation of perivascular brain capillary fibrinogen deposits negatively correlated with

loss of pericyte coverage (Fig. 1h,i), similar to that reported in pericyte-deficient mouse lines[5,41].

The analysis of the BBB tight junction proteins revealed loss in the zonula occludens-1 (ZO-1) and occludin length coverage in *APOE4* compared to *APOE3* mice both in the presence and absence of Aβ pathology (Fig. 1l,m). We found substantial 34% and 57% and 31% and 42% loss in ZO-1 length and 45% and 42% and 31% and 25% loss in occludin length in the cortex and hippocampus of *APOE3* and *APOE4* littermate controls alone and in these mice crossed with *5xFAD* mice, respectively (Fig. 1k,m). These findings were consistent with previously shown losses of the BBB tight junction proteins in *APOE4* (ref. [3]) and *5xFAD*[34] mice.

Cerebral blood flow reductions in *APOE4* and *APOE4*;*5xFAD* mice.

Next, we studied CBF changes in the cortex and hippocampus in 18–24-month-old *APOE3* and *APOE4* knock-in littermate controls and *APOE3;5xFAD* and *APOE4;5xFAD* mice, using a dynamic susceptibility-contrast (DSC)-MRI protocol as we previously developed[6,41]. We found that *APOE4* compared to *APOE3* mice develop a moderate, but substantial CBF loss in the cortex and hippocampus both in the presence and absence of Aβ pathology (Fig. 2a,b). This has been shown by 16% and 13% and 24% and 24% reductions in the regional cortical and hippocampal CBF in *APOE4* vs. *APOE3* mice alone and in these mice crossed with *5xFAD* mice, respectively (Fig. 2a,b). Additionally, we found substantial 23% and 23% and 31% and 33% reductions in the cortical and hippocampal CBF in *5xFAD* mice crossed to *APOE3* and *APOE4* mice compared to their respective knock-in littermate controls (Fig. 2b). As with BBB breakdown, sex did not have an effect on regional CBF changes in old mice (Extended Data Fig. 2).

Compared to *APOE3* mice, *APOE4* mice had also a moderate but substantial loss of capillary density in the cortex and hippocampus both in the presence and absence of Aβ pathology (Fig. 2c,d), as shown by 17% and 11% and 10% and 9% reductions in the cortical and hippocampal capillary length in *APOE4* versus *APOE3* littermate control mice and *APOE4;5xFAD* versus *APOE3;5xFAD* mice, respectively (Fig. 2d). CBF reductions positively correlated with reductions in the capillary length (Fig. 2e,f). The observed correlations were consistent with previously reported correlations between reductions in the CBF and microvascular density in pericyte-deficient[5,6,41] and *APOE4* (refs. [3,10]) mice.

Cyclophilin A-matrix metalloproteinase-9 pathway.

In a search of a mechanism underlying vascular changes in *APOE4* compared to the respective *APOE3* lines, we focused on the BBB-degrading pro-inflammatory cyclophilin A (CypA)-matrix metalloproteinase (MMP)-9 pathway. When activated by brain capillary pericytes in *APOE4* but not *APOE3* transgenic mice, this pathway leads to MMP9-mediated breakdown of the BBB via degradation of BBB tight junction proteins, which in turn leads to leakages of blood-derived toxic proteins causing neuronal stress and dysfunction[3]. Previous work using in vivo multiphoton microscopy of DQ-gelatin has shown increased gelatinase MMP cerebrovascular activity in *APOE4* compared to *APOE3* mice, which has been confirmed by gelatin zymography of brain tissue, demonstrating an increase in

pro-MMP9 and activated MMP9, but not MMP2 (ref. [3]).This pathway is also activated in human *APOE4* carriers diagnosed with AD, as suggested by neuropathological analysis[2] and in living human *APOE4* carriers, as shown by increased cerebrospinal fluid levels of CypA, MMP9 and sPDGFR-β, a marker of pericyte injury[17].

Immunocytochemical analysis indicated that *APOE4* mice compared to respective *APOE3* lines have higher levels of CypA+ immunofluorescent signal in CD13+ pericytes in the cortex and hippocampus both in the presence and absence of Aβ pathology (Fig. 3a,b). Specifically, we found 614% and 627% and 45% and 37% increases in CypA+ signal in the cortical and hippocampal pericytes in *APOE4* compared to *APOE3* control mice alone and in these mice crossed with *5xFAD* mice, respectively (Fig. 3b). Increases in the CypA+ immunofluorescent signal in CD13+ pericytes in the cortex and hippocampus in *APOE4* compared to *APOE3* mice without *5xFAD* transgenes (littermate controls) and with *5xFAD* transgenes both negatively correlated with the reduced length of the tight junction proteins ZO-1 (Fig. 3c,d) and occludin (Fig. 3e,f), but the effect was more pronounced in mice expressing *5xFAD* transgenes, as expected based on the signal intensity data.

We also found increased MMP9+ immunofluorescence signal in CD13+-pericytes (Fig. 3g,h) by 406% and 412% and 47% and 61% in the cortex and hippocampus in *APOE4* compared to *APOE3* control mice alone and in these mice crossed with *5xFAD* mice, respectively (Fig. 3h). Increases in the MMP9+ immunofluorescent signal in CD13+ pericytes in the cortex and hippocampus also negatively correlated with the reduced length of ZO-1 (Fig. 3i,j) and occludin (Fig. 3k,l), as determined by immunostaining on adjacent sections. As expected, there was a positive correlation between the CypA+ and MMP9+ immunofluorescent signals in CD13+ pericytes, both in the cortex and hippocampus, as shown by the correlation analysis using individual data points from both *APOE4* compared to *APOE3* mice without (littermate controls) and with *5xFAD* transgenes (Fig. 5m,n).

Altogether, these data demonstrate activation of the CypA-MMP9 pathway in pericytes in old *APOE4* and *APOE4;5xFAD* mice compared to the respective *APOE3* lines suggesting a possible mechanism for the *APOE4*-mediated BBB breakdown and loss of capillary density.

Aβ pathology and vascular dysfunction.

As previously reported[40], we also found that levels of Aβ42, the principal Aβ peptide in *5xFAD* mice[29,37], in the cortex and hippocampus were not substantially different between 18–24-month-old *APOE4;5xFAD* and *APOE3;5xFAD* mice (Fig. 4a). The tissue analysis confirmed comparable Aβ cortical and hippocampal load in these mice (Fig. 4b,c). As reported[40], Aβ42 levels in female *APOE3;5xFAD* and *APOE4;5xFAD* mice were substantially higher compared to the respective male mice (Fig. 4d). Consistent with previous reports in *5xFAD* lines[29,37], Aβ40 levels in both *APOE4;5xFAD* and *APOE3;5xFAD* mice were substantially lower than Aβ42 levels (Extended Data Fig. 3a). As with Aβ42, we also found substantially higher Aβ40 levels in female compared to male mice in both *APOE4* and *APOE3* mice crossed with *5xFAD* mice (Extended Data Fig. 3b).

Interestingly, the increased BBB permeability K_{trans} values and a moderate CBF loss in *APOE4* compared to *APOE3* mice crossed with *5xFAD* mice did not correlate with

elevated Aβ42 cortical or hippocampal levels (Fig. 4e–h) or Aβ40 levels (Extended Data Fig. 3e,f), suggesting that Aβ pathology is likely not causing vascular dysfunction in old *APOE4;5xFAD* when compared to *APOE3;5xFAD* mice.

APOE4-mediated neurodegeneration.

Next, we found that old *APOE4* mice compared to *APOE3* mice develop accelerated neuron and axon loss without and with Aβ pathology (Fig. 5a–f). This has been shown by 18% and 34% and 11% and 22% loss of neuronal counts and 20% and 27% and 27% and 43% decrease in the neuritic density in the cortex (Fig. 5b,c) and hippocampus (Fig. 5e,f) in *APOE4* versus *APOE3* control mice alone and in these mice crossed with *5xFAD* mice, respectively. Consistent with previous reports showing early neuronal dysfunction in *APOE4* transgenic lines[3] and in *5xFAD* mice showing neuron and synaptic loss[29,39], we found substantial 17% and 23% and 10% and 10% reduction in neuronal counts and 30% and 37% and 36% and 51% reduction in neuritic density in the cortex and hippocampus of *5xFAD;APOE3* and *5xFAD;APOE4* mice compared to their respective *APOE3* and *APOE4* knock-in littermate controls (Fig. 5b,c,e,f). Notably, loss of neurons correlated with the increased BBB K_{trans} values reflecting BBB breakdown (Fig. 5g,h), but did not correlate with elevated Aβ42 levels (Fig. 5i,j).

APOE4-related behavioral deficits.

Finally, we found that *APOE4* compared to *APOE3* mice develop behavioral deficits on daily activity tests as shown by a substantial drop in the nest construction score both in the presence and absence of Aβ pathology (Fig. 6a). A drop in the nesting scores correlated with the increased BBB K_{trans} values and diminished CBF (Fig. 6b–d), but did not correlate with elevated Aβ42 levels in the cortex or hippocampus (Fig. 6e,f). *APOE4* compared to *APOE3* mice also developed hippocampal-associated memory deficits as shown by their worse performance on the novel object location (NOL) test both in the presence and absence of Aβ pathology (Fig. 6g). Deficits in NOL exploratory preference correlated with the increased BBB permeability K_{trans} values in the hippocampus (Fig. 6h) and diminished CBF in the cortex (Fig. 6i), but not with elevated Aβ42 levels in either of these regions (Fig. 6j,k).

Inhibition of the CypA-MMP9 pathway in *APOE4;5FAD* mice.

Next, we treated 10–12-month-old *APOE4;5xFAD* and *APOE3;5xFAD* mice with a non-immunosuppressive CypA inhibitor Debio-025, which has been used in humans for non-neurological indications such as hepatitis C[46]. Additionally, Debio-025 is currently undergoing testing for SARS-CoV-2 infection[47] and is in phase 2 clinical trial against COVID-19 (www.clinicaltrialsarena.com/news/debiopharm-begins-alisporivir-france).

Debio-025 was administered for 30 d (10 mg kg^{-1} d^{-1} intraperitoneally (i.p.)) using a dosing regimen as previously reported in mouse models of muscular dystrophy and myopathy[48,49] and in the low-density lipoprotein receptor-related protein 1 (LRP1) endothelial-specific knockout mice[50]. We started Debio-025 at 10–12 months of age, when *APOE4;5xFAD* compared to *APOE3;5xFAD* mice develop accelerated BBB breakdown, behavioral deficits and substantial loss of neuronal networks, as reported[42,51] (Fig. 7a) The goal of this experiment was to determine whether protecting BBB integrity by suppressing the CypA-

MMP9 pathway in pericytes can prevent further neuron loss and behavioral changes in *APOE4;5xFAD* relative to *APOE3;5xFAD* mice.

Immunocytochemical analysis indicated that a 30-d treatment with Debio-025 compared to vehicle substantially reduced CypA$^+$ and MMP9$^+$ immunofluorescent signal in CD13$^+$ pericytes in the cortex and hippocampus of *APOE4;5xFAD* mice down to the levels seen in *APOE3;5xFAD* mice, respectively (Fig. 7b–e). Consistent with inhibition of the CypA-MMP9 BBB-degrading pathway[3], treatment of *APOE4;5xFAD* mice with Debio-025 increased the length coverage of tight junction proteins ZO-1 and occludin that are both well-known substrates for enzymatic degradation by MMP9 (ref. [3]) (Fig. 7f–i). However, Debio-025 did not have an effect on CypA$^+$ and/or MMP9$^+$ signal in CD13$^+$ pericytes, nor on ZO-1 and occludin length in *APOE3;5xFAD* mice. Inhibition of the CypA-MMP9 pathway in *APOE4;5xFAD* mice improved BBB integrity as shown in vivo by DCE-MRI (Fig. 7) and ex vivo by reduced perivascular capillary fibrinogen deposits (Fig. 7g) and was associated with improved pericyte coverage (Fig. 7h,i).

We then found that Debio-025 compared to vehicle prevented further loss of neurons and axon density in the cortex and hippocampus of *APOE4;5xFAD* mice (Fig. 8a–c) and improved performance on NOL and novel object recognition (NOR) hippocampal tests (Fig. 8d,e) bringing them nearly to the levels seen in *APOE3;5xFAD* mice, but did not have an effect on neuronal phenotype or behavior in *APOE3;5xFAD* mice. Notably, age-matched *APOE3* control mice not expressing *5xFAD* transgenes had still notably higher neuronal counts, neuritic density and better performance on hippocampal NOR test than Debio-025-treated *APOE4;5xFAD* mice or *APOE3;5xFAD* mice (Extended Data Fig. 4). These data suggest that Debio-025 ameliorates *APOE4*-mediated loss of neurons and behavioral deficits relative to *APOE3*, but does not protect against neurodegenerative changes caused by *5xFAD* transgenes and subsequent direct Aβ neurotoxicity, as previously shown in *5xFAD* mice[29,37,52]. Consistent with these findings, Debio-025 had no effect on Aβ42 or Aβ40 levels in the cortex and hippocampus of *APOE4;5xFAD* or *APOE3;5xFAD* mice (Fig. 8f,g), confirming that protection of neuronal phenotype in *APOE4;5xFAD* mice is independent of Aβ pathology.

Discussion

Our findings show that old *APOE4* knock-in mice and *APOE4;5xFAD* mice, compared to their respective *APOE3* lines develop an accelerated BBB breakdown associated with loss of pericyte capillary coverage and reductions in CBF associated with diminished capillary density both in the presence and absence of Aβ. Tissue analysis revealed reductions in the tight junction proteins ZO-1 and occludin coverage length, which correlated with activation of the CypA-MMP9 BBB-degrading pathway in pericytes. As previously reported, this pathway is activated in pericytes in substantial genic *APOE4* lines[3], as well as at the BBB endothelial cells and pericytes in human *APOE4* AD carriers as shown by postmortem tissue analysis[2] and in living *APOE4* carriers, as shown by cerebrospinal fluid analysis[17]. When activated, the CypA-MMP9 pathway leads to MMP9-mediated enzymatic degradation of the BBB tight junction proteins causing BBB breakdown[3,50].

As recently reported[40], we found comparable Aβ pathology in old *APOE3;5xFAD* and *APOE4;5xFAD* mice, but with higher severity in females than in males in both genotypes. Notably, elevated Aβ42 levels, the major Aβ species in *5xFAD* mice[29,30,37,40] and of Aβ40, did not correlate with BBB breakdown or CBF reductions in these mice, suggesting that *APOE4*-mediated vascular dysfunction in old mice is Aβ-independent. Moreover, neuron loss and behavioral deficits in *APOE4* compared to *APOE3* lines correlated well with losses in BBB integrity and CBF, but not with Aβ pathology, as indicated by the lack of correlation between neuron loss and Aβ42 levels, or behavioral deficits and Aβ42 levels.

Loss of neurons and neuritic density in *5xFAD* mice crossed with *APOE3* and *APOE4* mice is consistent with findings of neuron and synaptic loss in older *5xFAD* mice, as reported[29,39]. Strong correlation between BBB dysfunction and neurodegenerative and behavioral changes in *APOE4* compared to the respective *APOE3* lines, is consistent with enhanced brain capillary leakages of blood-derived neurotoxic proteins such as albumin[53], thrombin, plasminogen and/or iron-containing proteins[3,5] or fibrinogen[41], all capable of causing neuron and synaptic dysfunction and/or eventually neuron death by different but complementary mechanisms. Additionally, greater pericyte loss in *APOE4* compared to *APOE3* lines in the absence and presence of Aβ pathology results in a greater loss of pericyte-derived neurotrophic growth factors, such as pleiotrophin[6], which might further accelerate neuron loss particularly in the presence of diminished CBF, as we recently reported[6].

How different AD pathologies interact to contribute to an advanced AD disease stage with age has been understudied and poorly understood. The present findings indicate that vascular dysfunction, particularly the BBB breakdown, plays a important role accelerating neurodegenerative process and cognitive impairment in old Alzheimer's mice independently of Aβ and therefore it could be an important new therapeutic target for treating an advanced disease stage for which anti-Aβ strategies have proven to be ineffective. Indeed, treatment of *APOE4;5xFAD* mice with CypA inhibitor Debio-025 suppressed the CypA-MMP9 pathway in pericytes, which in turn improved BBB integrity and prevented further neuron loss and behavioral deficits despite having no effect on Aβ pathology. These results suggest that interventions directed at the BBB repair and improvement of vascular dysfunction are potentially viable new approaches to slow down and/or arrest neurodegenerative process and cognitive decline in an advanced AD stage. As Debio-025 has been used in humans for non-neurological applications[46] this approach may hold potential to treat cognitive impairment in *APOE4* carriers that show activation of the CypA-MMP9 pathway in the cerebrospinal at an early disease stage[17] and at the BBB at a later disease stage with fully developed AD as shown by neuropathological analysis[2].

One limitation of the present Debio-025 experiment, however, is that it has been performed in somewhat younger 10–12-month-old *APOE4;5xFAD* and *APOE3;5xFAD* mice, compared to the rest of the study that has been carried out in older 18–24-month-old mice. Although, at 10–12 months of age *APOE4;5xFAD* compared to *APOE3;5xFAD* mice develop accelerated BBB breakdown, behavioral deficits and notable loss of neuronal networks[42,51] and both genotypes develop substantial Aβ pathology[30,40], as we have also demonstrated, it remains to be seen whether Debio-025 treatment will have similar striking

effects in 18–24-month-old mice. This, however, is a challenging experiment because of increased mortality of *APOE4;5xFAD* mice at that old age as reported[40] and as we also observed.

Our data show that activation of the CypA-MMP9 pathway leads to reductions in tight junction proteins causing BBB breakdown in *APOE4* and *APOE4;5FAD* mice, but whether nonspecific caveolar transcytosis is also affected by *APOE4*, as in some other models of BBB breakdown[54], remains presently unknown and should be addressed by future studies. It has been also reported that epidermal growth factor (EGF) can increase capillary length and improve BBB permeability in *APOE4;5FAD* mice[42], but whether the EGF–EGFR signaling pathway can play a role in spontaneous BBB breakdown as observed in *APOE4;5FAD* mice has not been studied. Additionally, future studies should address at the cellular and molecular level how *APOE4* leads to CBF reductions and whether loss of CBF is related to loss in pericyte coverage and/or reductions in microvascular density, as suggested by our correlation data and/or is caused by activation of the CypA-MMP9 pathway in pericytes or alternatively by a different underlying mechanism.

The present study confirms that Aβ pathology increases BBB breakdown and CBF deficits in *APOE3;5xFAD* mice compared to *APOE3* control mice, which is to be expected given that *5xFAD* mice alone develop BBB breakdown[34–37] and CBF deficits[38], as a result of direct Aβ vasculotoxicity. Interestingly, we also found activation of the CypA–MMP9 pathway in pericytes in *APOE3;5xFAD* mice relative to *APOE3* control mice. Whether this could be attributed to direct toxic effects of Aβ on pericytes[43] and/or to Aβ-mediated proteasomal degradation of LRP1[55] resulting in loss of this receptor which is required for suppression of the CypA–MMP9 pathway by apoE3 (ref. [3]), remains to be determined by future studies. Namely, studies in pericyte cultures and transgenic mice show that apoE3 requires LRP1 to maintain CypA synthesis within low physiological range, whereas poor interaction of apoE4 with LRP1 in pericytes leads to activation of this pathway via transcriptional activation of CypA triggering NF-κB transcriptional activation of MMP9, which increases active MMP9 levels degrading BBB tight junction proteins[3]. Furthermore, silencing LRP1 in vivo in *APOE3* knock-in mice blocks apoE3-mediated suppression of CypA leading to activation of the CypA–MMP9 pathway and BBB breakdown similarly as seen in *APOE4* mice[3]. As LRP1 is reduced in blood vessels in AD in humans[2,55–57] and in AD Aβ models[55,58–60], it is possible that LRP1 loss from blood vessels and pericytes may contribute to activation of the CypA–MMP9 pathway in *APOE3;5xFAD* mice.

In conclusion, our findings show that *APOE4* accelerates advanced-stage vascular dysfunction, BBB breakdown and neurodegeneration in AD mice via the CypA pathway in pericytes independently of Aβ. These findings have implication not only for better understanding the pathogenesis of an advanced-stage vascular and neurodegenerative disorder in AD, but also for potential treatment of *APOE4* carriers with advanced AD for whom we do not have yet an effective apoE-based therapy to offer.

Methods

Animals.

As previously described[30], *APOE3;5xFAD* and *APOE4;5xFAD* mice, also commonly called *E3FAD* and *E4FAD* mice, respectively, were generated by crossing heterozygous *5xFAD*± line (Tg6799 on a C57BL/6 and SJL background) that coexpress five FAD mutations (*APP* K670N/M671L, I716V, V717I and *PS1* M146L, L286V) under the control of the neuron-specific mouse Thy-1 promoter[29] with homozygous human *APOE3*+/+ and *APOE4*+/+ targeted replacement mice (on C57BL/6 background)[28]. *APOE3;5xFAD* and *APOE4;5xFAD* littermate controls or noncarriers derived from these litters were *5xFAD*−/−*;APOE3*+/+ and *5xFAD*−/−*;APOE4*+/+, respectively, which we refer to as *APOE3* and *APOE4* knock-in control mice. Breeding pairs were generously provided by M. J. LaDu (University of Illinois at Chicago).

This study used both male and female mice at 18–24 months of age. The survival rate of mice at age 18 months was 90% and 80% for *APOE3* and *APOE4* knock-in littermate controls and 75% and 55% for *APOE3;5xFAD* and *APOE4;5xFAD* lines and was driven by early death of female *APOE4* mice, as previously shown[40]. All survivors between 18 and 24 months of age were used in the study. Group sizes varied from $n = 12$–16 for MRI studies, $n = 17$–25 for behavioral studies, $n = 14$–17 for Aβ assays and $n = 5$–6 for tissue immunohistology analysis for all four groups *APOE3*, *APOE4*, *APOE3;5xFAD* and *APOE4;5xFAD*. All procedures were approved by the Institutional Animal Care and Use Committee at the University of Southern California using US National Institutes of Health guidelines. All animals were randomized for their genotype information and were included in the study. The operators responsible for experimental procedure and data analysis were blinded and unaware of group allocation throughout the experiments.

Treatment with Debio-025.

Debio-025 (MedChem Express, cat. no. HY-12559), a non-immunosuppressive CypA inhibitor, was administered in 10–12-month-old *APOE3;5xFAD* and *APOE4;5xFAD* mice generated as above ($n = 7$–11 per group as indicated in Fig. 8 legend) at 10 mg kg^{-1} d^{-1} i.p. for 30 d following a dosing regimen as previously reported in mouse models[48–50]. Control mice received vehicle for 30 d. NOL and NOR behavioral tests were performed 30 d after Debio-025 or vehicle treatment before the DCE-MRI study. Mice were killed after 30 d and brains collected for tissue analysis.

Magnetic resonance imaging.

As we previously reported[6,41], mice were scanned with either a Biospec 7T system (300 MHz, Bruker) at the California Institute of Technology or a MR Solutions 7T positron emission tomography–MR system (MR Solutions Ltd.) at the Zilkha Neurogenetic Institute (University of Southern California). The Bruker system was equipped with the standard B-GA12 gradient set (~114-mm inner diameter; 400 mT.m^{-1} maximum gradient) and a 35-mm internal diameter quadrature volume coil (M2M Imaging). The MR Solutions system was equipped with the MRS cryogen-free MRI system (bore size ~24 mm, up to 600 mT.m^{-1} maximum gradient) and a 20-mm internal diameter quadrature bird cage mouse

head coil. Comparable sequences and parameters were used with both MR scanners, as described below.

As we previously reported [6,41], mice were anesthetized by 1–1.5% isoflurane/air. Respiration rate (80 ± 10 breaths min^{-1}) and body temperature (36.5 ± 0.5 °C) were monitored during the experiments using an abdominal pressure-sensitive probe and a rectal temperature probe. The isoflurane dose and heated air flow was adjusted continuously to ensure stable and reproducible depth of anesthesia. The sequences were collected in the following order: T2-weighted (two-dimensional-fast spin echo, TR/TE 4,900/45 ms, 34 slices, slice thickness 500 µm, in-plane resolution 70×70 µm^2) to obtain structural images; DCE protocol for the BBB permeability assessment; and finally, DSC imaging for CBF. Total imaging time was approximately 40 min per mouse.

As we previously reported[6,41], DCE-MRI imaging protocol was performed within the dorsal hippocampus territory and included measurement of pre-contrast T1-values using a variable flip angle fast low-angle shot (FLASH) sequence (FA= 5, 10, 15, 30 and 45°, TR/TE = 18 ms/4 ms, slice thickness 1 mm, in-plane resolution 85×85 µm^2), followed by a dynamic series of 325 T1-weighted images with identical geometry and a temporal resolution of 4.6 s (FLASH, TR/TE 18 ms/4 ms, flip angle 15°, slice thickness 1 mm, in-plane resolution 85×85 µm^2). Using a power injector, a bolus dose (140 µl) of 0.5 mmol kg^{-1} gadolinium-diethylenetriamine pentaacetic acid (Gd-DTPA), BioPAL, Inc., diluted in saline 1:6) was injected via the tail vein at a rate of 600 µl min^{-1}. DCE images were collected for 5 min before and 20 min after the injection. DSC-MRI imaging was performed on the exact same geometry. A dynamic series of 100 T2*-weighted images was used, with a temporal resolution of 1.5 s (FLASH, TR/TE 18 ms/4 ms, slice thickness 1 mm, flip angle 15°, in-plane resolution 170×270 µm^2). A second bolus dose (140 µl) of Gd-DTPA (1:1) was injected via the tail vein at a rate of 1,000 µl min^{-1}. DSC images were collected over 120 s after the injection.

MRI analysis.

T1 mapping.—As we described previously[6,41], T1 relaxation times were estimated using the variable flip angle method, before Gd-DTPA injection, with a series of FLASH images with varying FA and constant TR and TE using the standard saturation recovery equation.

Blood–brain barrier permeability.—As we previously reported[6,41], post-processing of the collected DCE-MRI data was performed using in-house DCE processing software (Rocketship) implemented in Matlab[61]. The unidirectional blood-to-brain transfer constant, K_{trans}, to intravenously injected gadolinium-based contrast agent was determined in both primary somatosensory cortex and hippocampus in mice using a modified method, as previously reported in both humans[17,23,26] and mice[6,41] with the post-processing Patlak analysis[62]. As reported previously[6,17,23,26,41], we determined the arterial input function (AIF) in each mouse from the common carotid artery.

As we previously reported[6,41], the total tracer concentration in the tissue, $C_{tissue}(t)$, can be described as a function of the arterial vascular concentration $C_{AIF}(t)$, the intravascular blood

volume v_p and the BBB permeability transfer constant K_{trans} that represents the flow of the tracer from the intravascular to the extravascular space using equation (1) below.

$$C_{tissue}(t) = K_{trans} \int_0^t C_{AIF}(\tau)d\tau + v_p \cdot C_{AIF}(t)$$

(1)

Cerebral blood flow.—As reported previously, DSC-MRI data were processed using our in-house Matlab code[6,41,63]. In brief, assuming a linear relationship between the signal drop induced by Gd-DTPA and concentration, these quantities can be related via:

$$S(t) = S_0 \times e^{-r2* \cdot C(t) \cdot TE}$$

(2)

Where $S(t)$ is the signal intensity at time t after bolus injection for any given voxel, S_0 is the mean pre-contrast signal intensity, r_2* relaxivity constant of the contrast agent used, $C(t)$ is the concentration of contrast as a function of time and TE is the time echo of the acquisition sequence. From the previous formula, the conversion from signal to contrast agent concentration is straightforward and occurs via:

$$C(t) = \frac{-1}{r_2* \cdot TE} \ln\left(\frac{S(t)}{S_0}\right)$$

(3)

As we previously reported[6,41], the profile of this concentration curve is heavily influenced by the manner in which the tracer bolus is injected into the mouse. To define the shape of the bolus curve, a representative AIF was obtained for each mouse individually. The AIF was obtained from the image data via manual delineation, typically from the common carotid arteries (same as for K_{trans} mapping). By defining the residual function, R(t), which represents the fraction of tracer presently circulating at time t, the relationship between tracer concentration and blood flow can be modeled as a convolution between R(t) and the AIF:

$$C_t(t) = \frac{\rho}{Kh} F \int_0^t C_a(\tau)R(t - \tau)d\tau$$

(4)

Where $C_t(t)$ is the concentration of contrast agent in the tissue, F is regional CBF, κ_H is the ratio of capillary to artery hematocrit (a value of 0.45 was used), ρ is tissue density (1.04 g ml^{-1}), $C_a(t)$ is AIF time course. To solve equation (4), we evoked an oscillation-limited circulant singular value decomposition approach[64]. Using this deconvolution, R(t) and F values were obtained and regional CBF (ml 100 g^{-1} min^{-1}) was computed using the equation:

$$\text{CBF} = \frac{\kappa_H}{\rho} \cdot \max(R(t)) \tag{5}$$

Behavior.

Nesting.—Nest construction test was performed as previously reported[41,43,59]. Two hours after the beginning of the dark cycle, the animals were individually placed in clean home cages with a single nestlet. Nests were assessed the next morning and evaluated following the five-point scale as we described in detail[59].

Novel object location.—This was performed as we have previously reported[5,6,43]. Briefly, animals were placed in a 30-cm^3 box and allowed to habituate to the testing area for 10 min. Animals were then placed back in their cages and two identical approximately 5 × 5-cm objects were placed in the top left and right corner of the testing area. Animals were allowed to explore the two objects in the testing area for 5 min before being returned to their cages. After a 1-h interval one of the objects was relocated and the animals were allowed to explore the testing area once again for 3 min. After each trial, the testing area and the objects were thoroughly cleaned with 70% ethanol solution. All the trials, including habituation, were recorded with a high-resolution camera and the amount of time each animal spent exploring the objects was analyzed. Any animals that presented a preference for either of the two identical objects, before replacement with the novel location, were eliminated from the analysis.

Immunohistochemistry.

As we previously reported[6,41], mice were anesthetized i.p. with 100 mg kg^{-1} ketamine and 10 mg kg^{-1} xylazine and transcardially perfused with 20 ml phosphate-buffered saline (PBS) containing 5 mM ethylenediaminetetraacetic acid (EDTA). Brains were removed, snap-frozen and one hemisphere was embedded into OCT compound (Tissue-Tek) on dry ice (the other hemisphere was used for biochemical assays; see Human Aβ40 and Aβ42 specific ELISA section). Brains were cryosectioned at a thickness of 20 μm and then fixed in 4% PFA as previously described. Sections were blocked with 5% normal donkey serum (Vector Laboratories)/0.1%Triton-X/0.01 M PBS for 1 h and incubated with primary antibodies diluted in blocking solution overnight at 4 °C. After incubation with primary antibodies, sections were washed in PBS and incubated with fluorophore-conjugated secondary antibodies (see below) and then mounted onto slides with fluorescence mounting medium (Dako). The following primary and secondary antibodies were used, respectively: for pericyte coverage, polyclonal goat anti-mouse aminopeptidase N/ANPEP (CD13) (R&D systems AF2335, 1:100 dilution) and Alexa Fluor 488- or 568-conjugated donkey anti-goat (Invitrogen, A-11055 or A-11057, 1:500 dilution); for fibrin/fibrinogen, polyclonal rabbit anti-human fibrinogen (Dako A0080, 1:500 dilution) and Alexa Fluor 488-conjugated donkey anti-rabbit (Invitrogen, A-21206,1:500 dilution); for tight junction proteins (zonula occludens), rabbit anti-mouse ZO-1 (Invitrogen 40–2200, 1:200 dilution) and Alexa Fluor 568-conjugated donkey anti-rabbit (Invitrogen A-10042, 1:500 dilution); and for occludin, mouse anti-mouse occludin (Invitrogen clone OC-3F10 no. 33–1500, 1:100 dilution) and

Alexa Fluor 488-conjugated donkey anti-mouse (Invitrogen A-21202, 1:500 dilution); for CypA, rabbit anti-mouse CypA (Abcam ab42408, 1:100 dilution) and Alexa Fluor 488 or 568-conjugated donkey anti-rabbit (Invitrogen A-21206 or A-10042, 1:500 dilution); for MMP9, rabbit anti-mouse MMP9 (Abcam, ab38898, 1:100 dilution) and Alexa Fluor 488 or 568-conjugated donkey anti-rabbit (Invitrogen A-21206 or A-10042, 1:500 dilution); for amyloid-β, rabbit anti-human β-amyloid (Cell Signaling 8243S, 1:500 dilution) and Alexa Fluor 647-conjugated donkey anti-rabbit (Invitrogen A-31573,1:500 dilution); for neurofilament, mouse monoclonal anti-axonal neurofilament marker (SMI312) (BioLegend SMI312, 1:500 dilution) and Alexa Fluor 488-conjugated donkey anti-mouse (Invitrogen A-21202, 1:500 dilution); and for neuronal, polyclonal rabbit anti-NeuN (Millipore ABN78, 1:500 dilution) and Alexa Fluor 488 or 568-conjugated donkey anti-rabbit (Invitrogen, A-21206 or A-10042; 1:500 dilution). To visualize brain microvessels, sections were incubated with Dylight 488, 594 or 647-conjugated *Lycopersicon esculentum* lectin (Vector Labs, DL-1174; 1:200 dilution) for 1 h. Sections were imaged with a Zeiss LSM 510 confocal laser-scanning microscope or BZ9000 fluorescence microscope. Z-stack projections and pseudo-coloring were performed using ZEN software (Carl Zeiss Microimaging). Image post-analysis was performed using ImageJ software.

Microscopy analysis.

For extravascular brain capillary leakages, pericyte coverage, tight junction protein analysis, CypA and MMP9 quantifications and NeuN+ neuron counts and neurofilament (SMI312) axons, 4–6 randomly selected fields in the somatosensory cortex region and/or the CA1 region of the hippocampus were analyzed for each animal in 3–4 nonadjacent sections (~100 μm apart) and averaged per mouse. For Aβ load, whole cortices and hippocampi were used, corresponding to the areas used for Aβ ELISA.

Extravascular leakages.—For detection of extravascular brain capillary fibrinogen deposits, an antibody that detects both fibrinogen and fibrinogen-derived fibrin polymers was used. Ten-micron maximum projection z-stacks were reconstructed and the fibrinogen+ perivascular signal on the abluminal side of lectin+ endothelial profiles on microvessels 6 μm in diameter was analyzed using ImageJ software Integrated density analysis measurement tool, as we previously described[41].

Pericyte coverage.—Ten-micron maximum projection z-stacks were reconstructed and the areas occupied by CD13+ pericytes on lectin+ endothelial profiles on microvessels 6 μm in diameter was analyzed using ImageJ as we previously described[65]

Immunofluorescent ZO-1 and occludin tight junction analysis.—The length of ZO-1+ and occludin+ immunofluorescent signal on lectin+ endothelial brain capillary profiles (<6 μm in diameter) in the cortex and the hippocampus was determined using the ImageJ Area measurement tool and expressed in mm of ZO-1 and occludin length per mm^2 of the total area of lectin+ endothelial capillary profiles, as we previously described[6].

Microvascular length.—Ten-micron maximum projection z-stacks were reconstructed and the length of lectin+ endothelial capillary profiles (6 μm in diameter) was measured

using the ImageJ plugin 'Neuro J' length analysis tool, as previously described[41,65]. The length was expressed in mm of lectin[+] endothelial capillary profiles per mm[3] of brain tissue.

Immunofluorescent CypA detection.—The area occupied by CypA^{+} immunofluorescent signal on CD13^{+} pericytes was expressed as the percentage of CD13^{+} pericyte area using the ImageJ Area measurement tool as we previously described[3]. Orthogonal views of confocal images of CypA, the pericyte marker CD13 and lectin^{+} endothelium showing colocalization of CypA with CD13^{+} pericytes were generated from a single-plane projection from a 20 single-plane z-stack using ZEN software (black edition). For the correlation analyses between CypA[+] pericytes and ZO-1 length and CypA[+] pericytes and occludin length immunostaining for CypA and CD13, ZO-1 and lectin-endothelial staining and occludin and lectin-endothelial staining was performed on adjacent sections.

Immunofluorescent MMP9 detection.—The area occupied by MMP9^{+} immunofluorescent signal on CD13^{+} pericytes was expressed as the percentage of CD13^{+} pericyte area using the ImageJ Area measurement tool as we previously described[3]. Orthogonal views of confocal images of MMP9, the pericyte marker CD13 and lectin^{+} endothelium showing colocalization of MMP9 with CD13^{+} pericytes were generated from a single-plane projection from a 20 single-plane z-stack using ZEN software (black edition). For the correlation analyses between MMP9^{+} pericytes and ZO-1 length and MMP9^{+} pericytes and occludin length immunostaining for MMP9 and CD13, ZO-1 and lectin-endothelial staining and occludin and lectin-endothelial staining was performed on adjacent sections.

Aβ load.—Primary somatosensory cortex and hippocampus were analyzed separately and the percentage area occupied by amyloid was quantified using Otsu-thresholding in ImageJ, as previously described[37].

NeuN[+] neuronal nuclei counting.—NeuN^{+} neurons were quantified using the ImageJ Cell Counter analysis tool, as previously described[6].

Neurofilament (SMI312)[+] axons.—As we previously described[6,41], 10-μm maximum projection z-stacks were reconstructed and SMI312^{+} signal was subjected to threshold processing and analysis using ImageJ.

Human Aβ40 and Aβ42 ELISA.

Cortices and hippocampi were isolated and snap-frozen from one brain hemisphere (the other hemisphere was used for immunohistochemical assays; see Immunohistochemistry section). Cortices and hippocampi were sequentially extracted with sonication, first extracted with ten volumes of Tris-buffered saline with complete protease inhibitor cocktail (Roche), centrifuged at $20,000g$ for 30 min at 4 °C, followed by homogenization of pellet in ice-cold guanidine buffer (5 M guanidine hydrochloride/50 mM Tris HCl, pH 8). Guanidine extracts were diluted 1:200 and 1:20,000 for measurement of human Aβ40 and Aβ42, respectively by a Meso Scale Discovery assay (K15200E-1).

Statistical analysis.

Sample sizes were calculated using nQUERY assuming a two-sided α-level of 0.05, 80% power and homogeneous variances for the samples to be compared, with the means and common s.d. for different parameters predicted from published data and our previous studies. For comparison between two groups, an *F* test was conducted to determine the similarity in the variances between the groups that are statistically compared and statistical significance was analyzed by unpaired two-tailed Student's *t*-test. Lilliefors test was used to test normality of the data (XLSTAT). For multiple comparisons, the *F* test was also used to determine the equality of variances between the groups compared and one-way ANOVA followed by Tukey's post hoc test, which was used to test statistical significance. For correlation analyses, we employed Pearson's correlation coefficient to measure the strength of the linear relationship between two variables. All analyses were performed using GraphPad Prism v.8.4.2 software and by an investigator blinded to the experimental conditions. Data are presented as violin plots with median and interquartile range as indicated in figure legends. A *P* value >0.05 was considered statistically not significant.

Reporting Summary.

Further information on research design is available in the Nature Research Reporting Summary linked to this article.
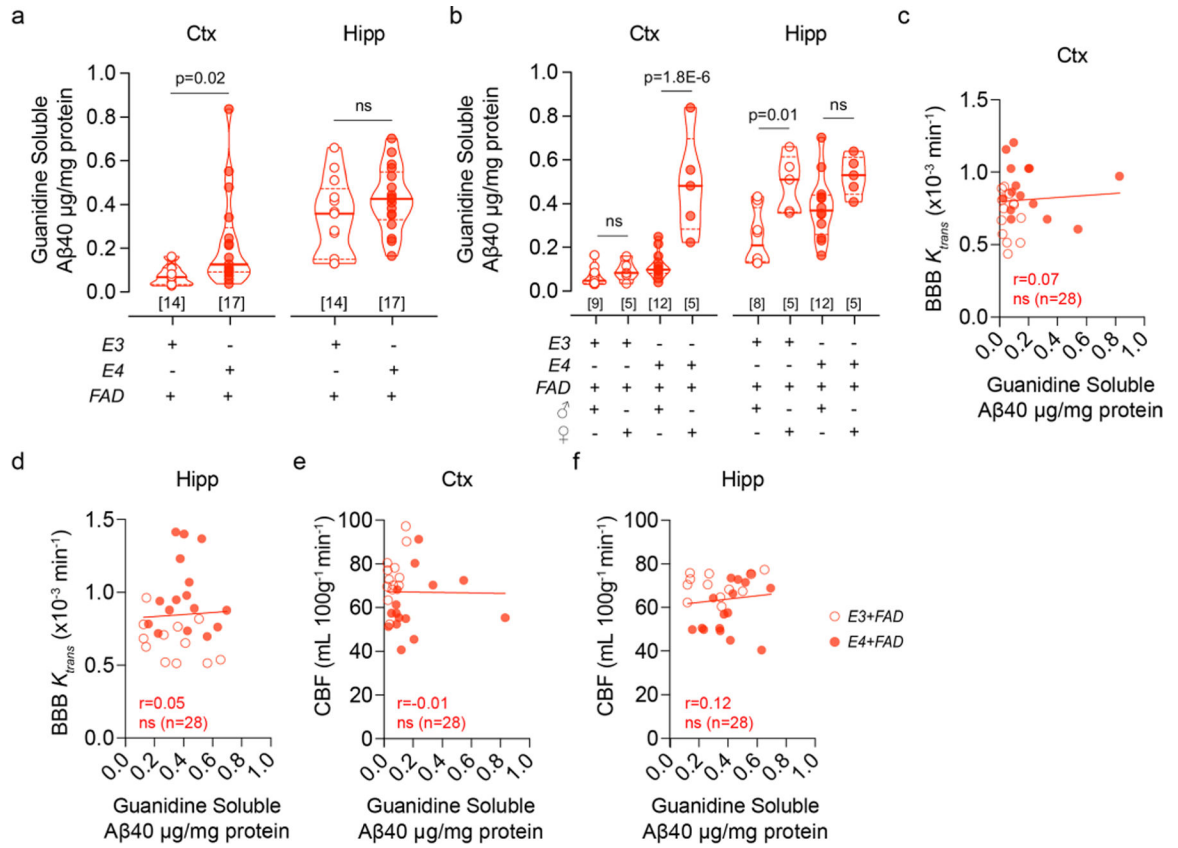
Extended Data
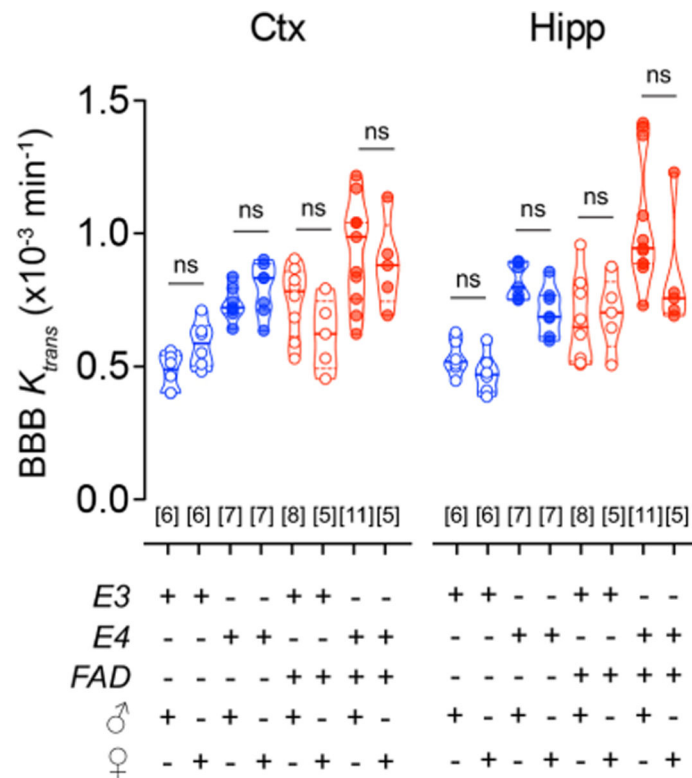
Extended Data Fig. 1 |. Additional characterization of blood-brain barrier breakdown in old *APOE4* and *APOE4;5xFAD* male and female mice.

Blood-brain barrier (BBB) permeability K_{trans} values in the cortex (Ctx) and hippocampus (Hipp) in male and female *E3* (n = 12, 6 ♂ and 6 ♀; blue empty circles), *E4* (n = 14, 7 ♂ and 7 ♀; blue filled circles), *E3+FAD* (n = 13, 8 ♂ and 5 ♀; red empty circles), and *E4+FAD* (n = 16, 11 ♂ and 5 ♀; red filled circles) mice generated from dynamic contrast-enhanced magnetic resonance scans. Mice (both genders) were 18–24-month old. Data are presented as truncated violin plots; continuous line, median; dotted line, interquartile range. Significance by one-way ANOVA followed by the Tukey post hoc test; ns, non-significant.
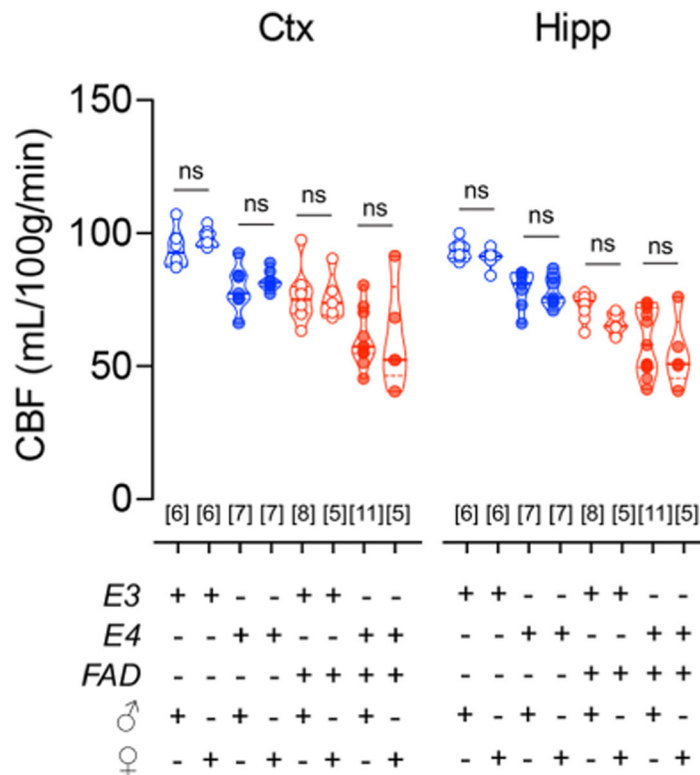
Extended Data Fig. 2 |. Additional characterization of cerebral blood flow reductions in old *APOE4* and *APOE4*;*5xFAD* male and female mice.
Cerebral blood flow (CBF) values in the cortex (Ctx) and hippocampus (Hipp) in male and female *E3* (n = 12, 6 ♂ and 6 ♀; blue empty circles), *E4* (n = 14, 7 ♂ and 7 ♀; blue filled circles), *E3+FAD* (n = 13, 8 ♂ and 5 ♀; red empty circles), and *E4+FAD* (n = 16, 11 ♂ and 5 ♀; red filled circles) mice generated from dynamic susceptibility-contrast magnetic resonance scans. Mice (both genders) were 18–24-month old. Data are presented as truncated violin plots; continuous line, median; dotted line, interquartile range. Significance by one-way ANOVA followed by the Tukey post hoc test; ns, non-significant.

Extended Data Fig. 3 |. Additional characterization of Aβ pathology in old *APOE3;5xFAD* and *APOE4;5xFAD* male and female mice and Aβ-independent vascular changes.
a Aβ40 levels in the Ctx and Hipp in *E3+FAD* (n = 14) and *E4+FAD* (n = 17) mice. **b**, Aβ40 levels in the Ctx and Hipp in male and female *E3+FAD* (n = 13–14, 8–9 ♂ and 5 ♀) and *E4+FAD* (n = 17, 12 ♂ and 5 ♀) mice. Data are presented as truncated violin plots; continuous line, median; dotted line, interquartile range. **c-f,** Lack of correlation between the blood-brain barrier (BBB) permeability K_{trans} values and Aβ40 levels in the Ctx and Hipp (**c,d**) and regional cerebral blood flow (CBF) values and Aβ40 levels in the Ctx and Hipp (**e,f**). Mice (both genders) were 18–24-month old (n = 28 individual points from both groups). In **a**, significance by unpaired two-tailed Student *t*-tests. In **b**, significance by one-way ANOVA followed by the Tukey post hoc test. In **c-f**, significance by two-tailed simple linear regression; r, Pearson correlation; ns, non-significant.
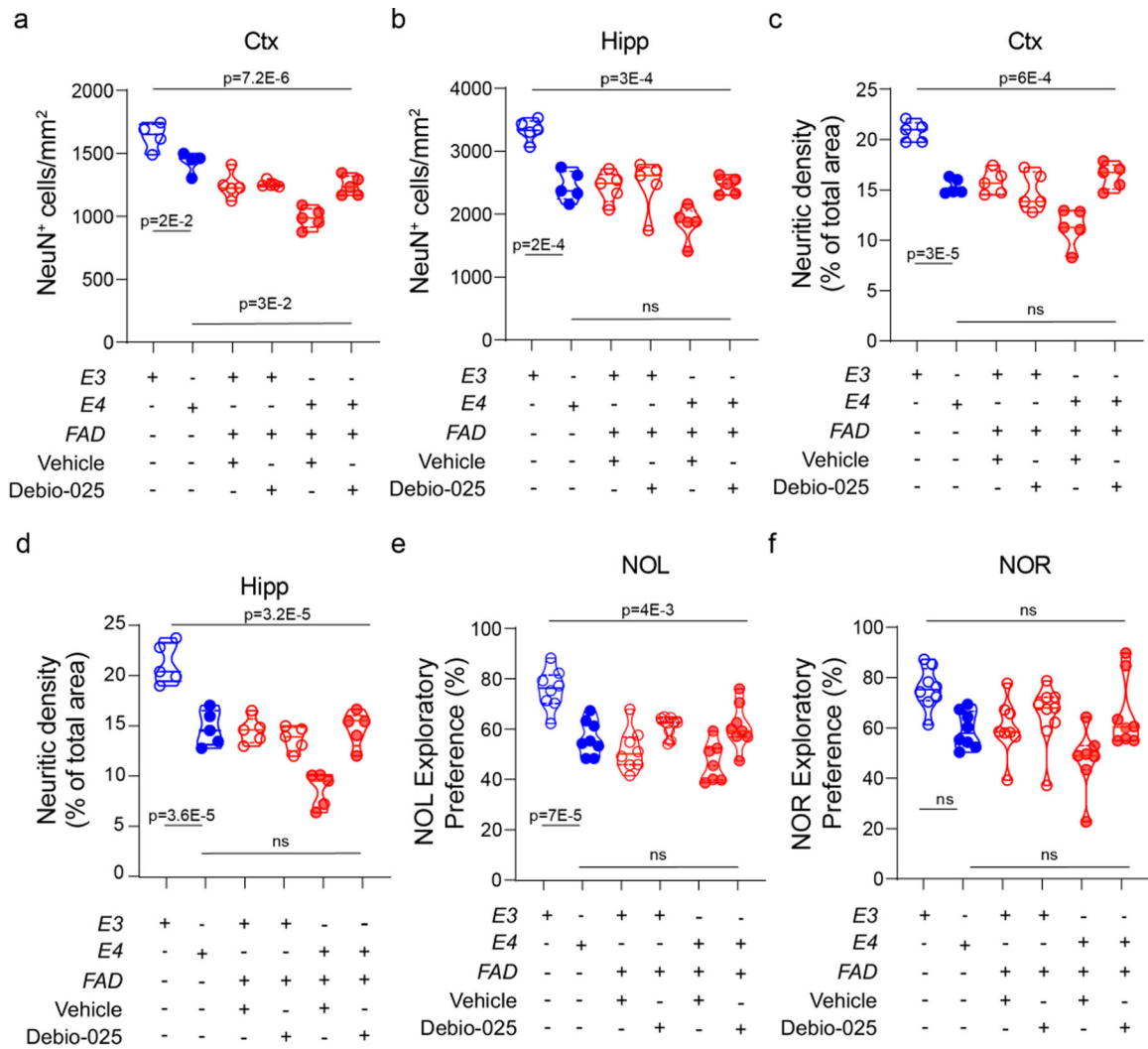
Extended Data Fig. 4 |. Effects of Debio-025 relative to vehicle on neuron counts, neuritic density and behavior in *APOE4;5xFAD* and *APOE3;5xFAD* mice (red circles, data taken from Fig. 8) compared to the littermate controls without *5XFAD* transgenes (blue circles).

a–d, Quantification of NeuN+-neurons (**a,b**) and SMI312+-neuritic density (**c,d**) in the Ctx and Hipp in *E3* (blue empty circles) and *E4* (blue filled circles) untreated littermate controls without *5xFAD* transgenes compared to age-matched *E3*+*FAD* (red empty circles) and *E4*+*FAD* (red filled circles) mice treated with vehicle or Debio-025; In **a-d**, n = 5 mice per group except in **a**. n = 4 in for *E3* littermate controls without *5XFAD* transgenes.

e,f, Novel object location (NOL; **e**) and novel object recognition (NOR; **f**) in *E3* (n = 8, blue empty circles) and *E4* (n = 8, blue filled circles) untreated littermate controls without *5XFAD* transgenes compared to age-matched *E3*+*FAD* vehicle-treated (n = 8; red empty circles), *E3*+*FAD* Debio-025-treated (n = 9; red empty circles), *E4*+*FAD* vehicle-treated (n = 7; red filled circles), and *E4*+*FAD* Debio-025-treated (n = 8; red filled circles) mice. Mice (both genders) were 10–12-month-old. In all graphs, data for *E3*+*FAD* and *E4*+*FAD* animals are the same as in Fig. 8 (red circles empty and filled); new data used for comparison are from their respective untreated littermate controls without *5XFAD* transgenes (blue circles

empty and filled). All data are presented as violin plots; continuous line, median; dotted line, interquartile range. Significance by one-way ANOVA followed by the Tukey post hoc test.

Acknowledgements

References

1. Yamazaki Y, Zhao N, Caulfield TR, Liu CC & Bu G Apolipoprotein E and Alzheimer disease: pathobiology and targeting strategies. Nat. Rev. Neurol 15, 501–518 (2019). [PubMed: 31367008]

2. Halliday MR et al. Accelerated pericyte degeneration and blood–brain barrier breakdown in apolipoprotein E4 carriers with Alzheimer's disease. J. Cereb. Blood Flow Metab 36, 216–227 (2016). [PubMed: 25757756]

3. Bell RD et al. Apolipoprotein E controls cerebrovascular integrity via cyclophilin A. Nature 485, 512–516 (2012). [PubMed: 22622580]

4. Armulik A et al. Pericytes regulate the blood–brain barrier. Nature 468, 557–561 (2010). [PubMed: 20944627]

5. Bell RD et al. Pericytes control key neurovascular functions and neuronal phenotype in the adult brain and during brain aging. Neuron 68, 409–427 (2010). [PubMed: 21040844]

6. Nikolakopoulou AM et al. Pericyte loss leads to circulatory failure and pleiotrophin depletion causing neuron loss. Nat. Neurosci 22, 1089–1098 (2019). [PubMed: 31235908]

7. Thambisetty M, Beason-Held L, An Y, Kraut MA & Resnick SM APOE epsilon4 genotype and longitudinal changes in cerebral blood flow in normal aging. Arch. Neurol 67, 93–98 (2010). [PubMed: 20065135]

8. Michels L et al. Arterial spin labeling imaging reveals widespread and Aβ-independent reductions in cerebral blood flow in elderly apolipoprotein epsilon-4 carriers. J. Cereb. Blood Flow Metab 36, 581–595 (2016). [PubMed: 26661143]

9. Reiman EM et al. Functional brain abnormalities in young adults at genetic risk for late-onset Alzheimer's dementia. Proc. Natl Acad. Sci. USA 101, 284–289 (2004). [PubMed: 14688411]

10. Koizumi K et al. Apoepsilon4 disrupts neurovascular regulation and undermines white matter integrity and cognitive function. Nat. Commun 9, 3816 (2018). [PubMed: 30232327]

11. Mahley RW & Huang Y Apolipoprotein E sets the stage: response to injury triggers neuropathology. Neuron 76, 871–885 (2012). [PubMed: 23217737]

12. Shi Y et al. ApoE4 markedly exacerbates tau-mediated neurodegeneration in a mouse model of tauopathy. Nature 549, 523–527 (2017). [PubMed: 28959956]

13. Deane R et al. apoE isoform-specific disruption of amyloid β peptide clearance from mouse brain. J. Clin. Invest 118, 4002–4013 (2008). [PubMed: 19033669]

14. Huynh TV, Davis AA, Ulrich JD & Holtzman DM Apolipoprotein E and Alzheimer's disease: the influence of apolipoprotein E on amyloid-β and other amyloidogenic proteins. J. Lipid Res 58, 824–836 (2017). [PubMed: 28246336]

15. Holtzman DM et al. Apolipoprotein E isoform-dependent amyloid deposition and neuritic degeneration in a mouse model of Alzheimer's disease. Proc. Natl Acad. Sci. USA 97, 2892–2897 (2000). [PubMed: 10694577]

16. Hudry E et al. Gene transfer of human Apoe isoforms results in differential modulation of amyloid deposition and neurotoxicity in mouse brain. Sci. Transl. Med 5, 212ra161 (2013).

17. Montagne A et al. APOE4 leads to blood–brain barrier dysfunction predicting cognitive decline. Nature 581, 71–76 (2020). [PubMed: 32376954]

18. Wardlaw JM et al. Neuroimaging standards for research into small vessel disease and its contribution to ageing and neurodegeneration. Lancet Neurol 12, 822–838 (2013). [PubMed: 23867200]

19. Kapasi A, DeCarli C & Schneider JA Impact of multiple pathologies on the threshold for clinically overt dementia. Acta Neuropathol 134, 171–186 (2017). [PubMed: 28488154]

20. Iturria-Medina Y et al. Early role of vascular dysregulation on late-onset Alzheimer's disease based on multifactorial data-driven analysis. Nat. Commun 7, 11934 (2016). [PubMed: 27327500]

21. Sweeney MD et al. Vascular dysfunction: the disregarded partner of Alzheimer's disease. Alzheimers Dement 15, 158–167 (2019). [PubMed: 30642436]

22. Iadecola C The neurovascular unit coming of age: a journey through neurovascular coupling in health and disease. Neuron 96, 17–42 (2017). [PubMed: 28957666]

23. Montagne A et al. Blood–brain barrier breakdown in the aging human hippocampus. Neuron 85, 296–302 (2015). [PubMed: 25611508]

24. van de Haar HJ et al. Neurovascular unit impairment in early Alzheimer's disease measured with magnetic resonance imaging. Neurobiol. Aging 45, 190–196 (2016). [PubMed: 27459939]

25. van de Haar HJ et al. Blood–Brain barrier leakage in patients with early Alzheimer disease. Radiology 281, 527–535 (2016). [PubMed: 27243267]

26. Nation DA et al. Blood–brain barrier breakdown is an early biomarker of human cognitive dysfunction. Nat. Med 25, 270–276 (2019). [PubMed: 30643288]

27. Jack CR Jr. et al. NIA-AA research framework: toward a biological definition of Alzheimer's disease. Alzheimers Dement 14, 535–562 (2018). [PubMed: 29653606]

28. Sullivan PM et al. Targeted replacement of the mouse apolipoprotein E gene with the common human APOE3 allele enhances diet-induced hypercholesterolemia and atherosclerosis. J. Biol. Chem 272, 17972–17980 (1997). [PubMed: 9218423]

29. Oakley H et al. Intraneuronal β-amyloid aggregates, neurodegeneration, and neuron loss in transgenic mice with five familial Alzheimer's disease mutations: potential factors in amyloid plaque formation. J. Neurosci 26, 10129–10140 (2006). [PubMed: 17021169]

30. Youmans KL et al. APOE4-specific changes in Aβ accumulation in a new transgenic mouse model of Alzheimer disease. J. Biol. Chem 287, 41774–41786 (2012). [PubMed: 23060451]

31. Nishitsuji K, Hosono T, Nakamura T, Bu G & Michikawa M Apolipoprotein E regulates the integrity of tight junctions in an isoform-dependent manner in an in vitro blood–brain barrier model. J. Biol. Chem 286, 17536–17542 (2011). [PubMed: 21471207]

32. Alata W, Ye Y, St-Amour I, Vandal M & Calon F Human apolipoprotein E varepsilon4 expression impairs cerebral vascularization and blood–brain barrier function in mice. J. Cereb. Blood Flow Metab 35, 86–94 (2015). [PubMed: 25335802]

33. Cacciottolo M et al. The APOE4 allele shows opposite sex bias in microbleeds and Alzheimer's disease of humans and mice. Neurobiol. Aging 37, 47–57 (2016). [PubMed: 26686669]

34. Kook SY et al. Aβ(1)(−)(4)(2)-RAGE interaction disrupts tight junctions of the blood–brain barrier via Ca(2)(+)-calcineurin signaling. J. Neurosci 32, 8845–8854 (2012). [PubMed: 22745485]

35. Giannoni P et al. Cerebrovascular pathology during the progression of experimental Alzheimer's disease. Neurobiol. Dis 88, 107–117 (2016). [PubMed: 26774030]

36. Park JC et al. Annexin A1 restores Aβ1–42 -induced blood–brain barrier disruption through the inhibition of RhoA-ROCK signaling pathway. Aging Cell 16, 149–161 (2017). [PubMed: 27633771]

37. Lazic D et al. 3K3A-activated protein C blocks amyloidogenic BACE1 pathway and improves functional outcome in mice. J. Exp. Med 216, 279–293 (2019). [PubMed: 30647119]

38. Eguchi K et al. Whole-brain low-intensity pulsed ultrasound therapy markedly improves cognitive dysfunctions in mouse models of dementia: crucial roles of endothelial nitric oxide synthase. Brain Stimul 11, 959–973 (2018). [PubMed: 29857968]

39. Neuman KM et al. Evidence for Alzheimer's disease-linked synapse loss and compensation in mouse and human hippocampal CA1 pyramidal neurons. Brain Struct. Funct 220, 3143–3165 (2015). [PubMed: 25031178]

40. Balu D et al. The role of APOE in transgenic mouse models of AD. Neurosci. Lett 707, 134285 (2019). [PubMed: 31150730]

41. Montagne A et al. Pericyte degeneration causes white matter dysfunction in the mouse central nervous system. Nat. Med 24, 326–337 (2018). [PubMed: 29400711]

42. Thomas R et al. Epidermal growth factor prevents APOE4 and amyloid-β-induced cognitive and cerebrovascular deficits in female mice. Acta Neuropathol. Commun 4, 111 (2016). [PubMed: 27788676]

43. Sagare AP et al. Pericyte loss influences Alzheimer-like neurodegeneration in mice. Nat. Commun 4, 2932 (2013). [PubMed: 24336108]

44. Park L et al. Innate immunity receptor CD36 promotes cerebral amyloid angiopathy. Proc. Natl Acad. Sci. USA 110, 3089–3094 (2013). [PubMed: 23382216]

45. Park L et al. Age-dependent neurovascular dysfunction and damage in a mouse model of cerebral amyloid angiopathy. Stroke 45, 1815–1821 (2014). [PubMed: 24781082]

46. Stanciu C, Trifan A, Muzica C & Sfarti C Efficacy and safety of alisporivir for the treatment of hepatitis C infection. Expert Opin. Pharmacother 20, 379–384 (2019). [PubMed: 30576256]

47. Softic L et al. Inhibition of SARS-CoV-2 infection by the cyclophilin inhibitor alisporivir (Debio 025). Antimicrob. Agents Chemother 64, e00876–20 (2020). [PubMed: 32376613]

48. Millay DP et al. Genetic and pharmacologic inhibition of mitochondrial-dependent necrosis attenuates muscular dystrophy. Nat. Med 14, 442–447 (2008). [PubMed: 18345011]

49. Tiepolo T et al. The cyclophilin inhibitor Debio 025 normalizes mitochondrial function, muscle apoptosis and ultrastructural defects in Col6a1$^{-/-}$myopathic mice. Br. J. Pharmacol 157, 1045–1052 (2009). [PubMed: 19519726]

50. Nikolakopoulou AM et al. Endothelial LRP1 protects against neurodegeneration by blocking cyclophilin A. J. Exp. Med 218, e20202207 (2021). [PubMed: 33533918]

51. Tai LM et al. EFAD transgenic mice as a human APOE relevant preclinical model of Alzheimer's disease. J. Lipid Res 58, 1733–1755 (2017). [PubMed: 28389477]

52. Eimer WA & Vassar R Neuron loss in the 5XFAD mouse model of Alzheimer's disease correlates with intraneuronal Aβ42 accumulation and caspase-3 activation. Mol. Neurodegener 8, 2 (2013). [PubMed: 23316765]

53. Senatorov VV Jr. et al. Blood–brain barrier dysfunction in aging induces hyperactivation of TGFβ signaling and chronic yet reversible neural dysfunction. Sci. Transl. Med 11, eaaw8283 (2019). [PubMed: 31801886]

54. Andreone BJ et al. Blood–brain barrier permeability is regulated by lipid transport-dependent suppression of caveolae-mediated transcytosis. Neuron 94, 581–594 (2017). [PubMed: 28416077]

55. Deane R et al. LRP/amyloid β-peptide interaction mediates differential brain efflux of Aβ isoforms. Neuron 43, 333–344 (2004). [PubMed: 15294142]

56. Shibata M et al. Clearance of Alzheimer's amyloid-ss(1–40) peptide from brain by LDL receptor-related protein-1 at the blood–brain barrier. J. Clin. Invest 106, 1489–1499 (2000). [PubMed: 11120756]

57. Donahue JE et al. RAGE, LRP-1, and amyloid-β protein in Alzheimer's disease. Acta Neuropathol 112, 405–415 (2006). [PubMed: 16865397]

58. Zhao Z et al. Central role for PICALM in amyloid-β blood–brain barrier transcytosis and clearance. Nat. Neurosci 18, 978–987 (2015). [PubMed: 26005850]

59. Winkler EA et al. GLUT1 reductions exacerbate Alzheimer's disease vasculo-neuronal dysfunction and degeneration. Nat. Neurosci 18, 521–530 (2015). [PubMed: 25730668]

60. Jaeger LB et al. Testing the neurovascular hypothesis of Alzheimer's disease: LRP-1 antisense reduces blood–brain barrier clearance, increases brain levels of amyloid-β protein, and impairs cognition. J. Alzheimers Dis 17, 553–570 (2009). [PubMed: 19433890]

61. Barnes SR et al. ROCKETSHIP: a flexible and modular software tool for the planning, processing and analysis of dynamic MRI studies. BMC Med. Imaging 15, 19 (2015). [PubMed: 26076957]

62. Barnes SR et al. Optimal acquisition and modeling parameters for accurate assessment of low Ktrans blood–brain barrier permeability using dynamic contrast-enhanced MRI. Magn. Reson. Med 75, 1967–1977 (2016). [PubMed: 26077645]

63. Ostergaard L, Weisskoff RM, Chesler DA, Gyldensted C & Rosen BR High resolution measurement of cerebral blood flow using intravascular tracer bolus passages. Part I: mathematical approach and statistical analysis. Magn. Reson. Med 36, 715–725 (1996). [PubMed: 8916022]

64. Wu O et al. Tracer arrival timing-insensitive technique for estimating flow in MR perfusion-weighted imaging using singular value decomposition with a block-circulant deconvolution matrix. Magn. Reson. Med 50, 164–174 (2003). [PubMed: 12815691]

65. Nikolakopoulou AM, Zhao Z, Montagne A & Zlokovic BV Regional early and progressive loss of brain pericytes but not vascular smooth muscle cells in adult mice with disrupted platelet-derived growth factor receptor-β signaling. PLoS ONE 12, e0176225 (2017). [PubMed: 28441414]
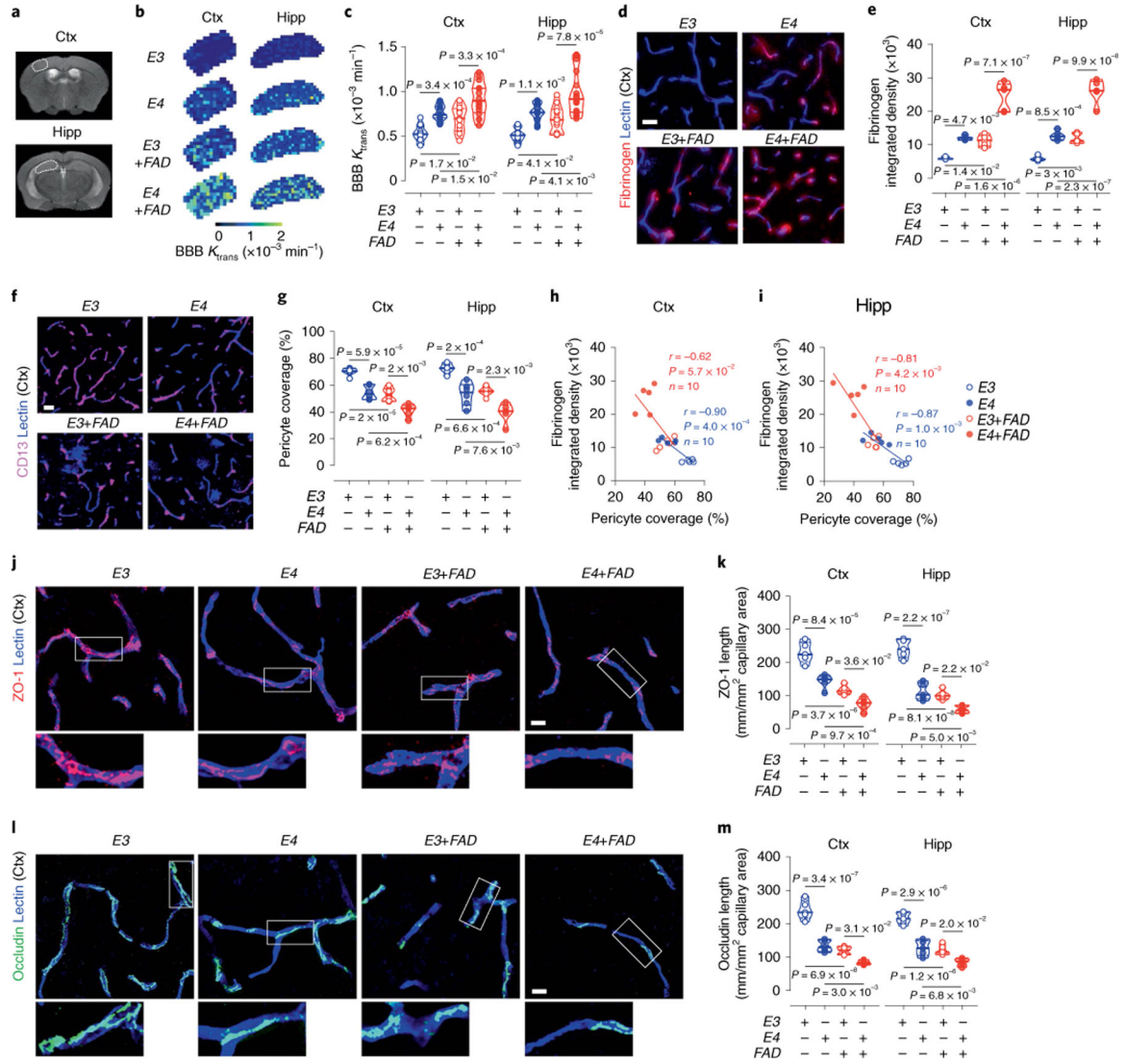
Fig. 1 |. Blood–brain barrier breakdown in old *APOE4* and *APOE4;5xFAD* mice.
a, T2-weighted scans displaying regions of interest: primary somatosensory cortex (Ctx) and hippocampus (Hipp). **b,c,** Representative K_{trans} maps (**b**) and BBB permeability K_{trans} values (**c**) in the Ctx and Hipp in *APOE3* (*E3*, $n = 12$; blue empty circles), *APOE4* (*E4*, $n = 14$; blue-filled circles), *APOE3;5xFAD* (*E3+FAD*, $n = 13$; red empty circles) and *APOE4;5xFAD* (*E4+FAD*, $n = 16$; red-filled circles) mice generated from DCe-MRI scans. **d,e,** Fibrinogen+ perivascular capillary deposits (red) in the Ctx (**d**) and quantification of fibrinogen+ deposits in the Ctx and Hipp (**e**) in *E3*, *E4*, *E3+FAD* and *E4+FAD* mice. Blue, lectin+ endothelial profiles; $n = 5$ mice per group; scale bar, 20 μm. **f,g,** CD13+ pericyte coverage (magenta) of lectin+ endothelial capillary profiles (blue) in the Ctx (**f**) and quantification of pericyte coverage on capillaries in the Ctx and Hipp (**g**) in *E3* ($n = 6$), *E4* ($n = 6$), *E3+FAD* ($n = 6$) and *E4+FAD* ($n = 5$) mice; scale bar, 20 μm. **h,i,** Negative correlation between fibrinogen deposits and pericyte coverage in the Ctx (**h**) and Hipp (**i**) using individual mouse data points from the studied groups. Mice (both sexes) were 18–24 months old. **j–m,** Representative immunostaining for ZO-1 (red) and lectin+ endothelium

(blue) in the Ctx (**l**, red) and ZO-1 length in the Ctx and Hipp (**k**) and immunostaining for occludin (green) and lectin[+] endothelium (blue) in the Ctx (**l**, green) and occludin length in the Ctx and Hipp (**m**) in *E3* (blue empty circles), *E4* (blue-filled circles), *E3*[+]*FAD* (red empty circles) and *E4*[+]*FAD* (red-filled circles) mice; $n = 5$ mice/group; scale bar, 20 μm. Boxes in **j** and **l** denote sites taken for higher magnification insets shown below merged images. Mice (both sexes) were 18–24 months old. In **c,e,g,k** and **m** data are presented as truncated violin plots; continuous line, median; and dotted line, interquartile range. Significance by one-way analysis of variance (ANOVA) followed by the Tukey post hoc test. Significance by two-tailed simple linear regression (**h,i**); *r*, Pearson correlation coefficient.
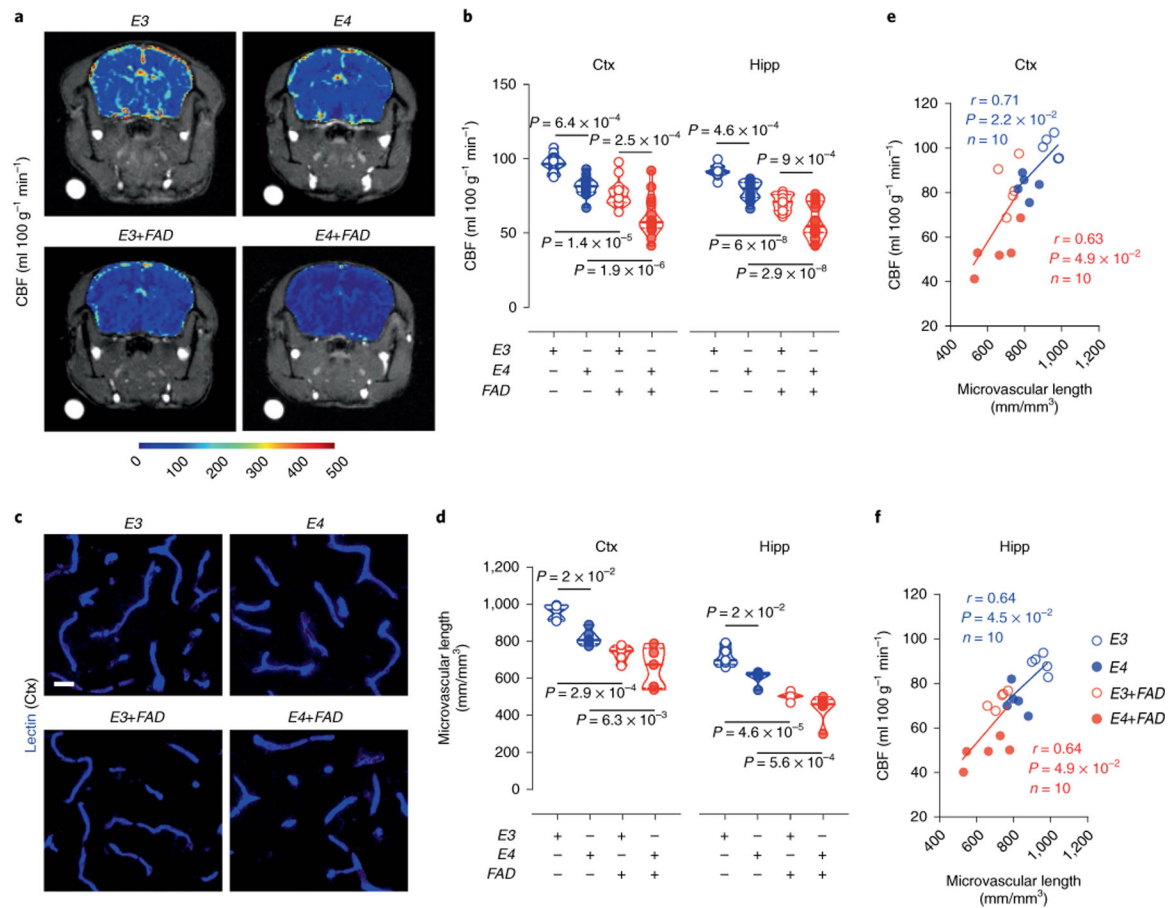
Fig. 2 |. Cerebral blood flow reductions in old *APOE4* and *APOE4*;*5xFAD* mice.
a,**b**, Representative CBF maps (**a**) and regional CBF values (**b**) in the cortex (Ctx) and hippocampus (Hipp) in *E3* (*n* = 12; blue empty circles), *E4* (*n* = 14; blue-filled circles), *E3*⁺*FAD* (*n* = 13; red empty circles) and *E4*⁺*FAD* (*n* = 16; red-filled circles) mice generated from dynamic susceptibility-contrast magnetic resonance scans. **c**,**d**, Representative lectin⁺ endothelial profiles (blue) in the Ctx (**c**) and microvascular length in the Ctx and Hipp (**d**) in *E3*, *E4*, *E3*⁺*FAD* and *E4*⁺*FAD* mice; *n* = 5 mice/group; scale bar, 20 μm. **e**,**f**, Positive correlation between the CBF and microvascular length in the Ctx (**e**) and Hipp (**f**) using individual mouse data points from the studied groups. Mice (both sexes) were 18–24 months old. In **b** and **d**, data are presented as truncated violin plots; continuous line, median; and dotted line, interquartile range. Significance by one-way ANOVA followed by the Tukey post hoc test. In **e** and **f**, significance was determined by two-tailed simple linear regression.
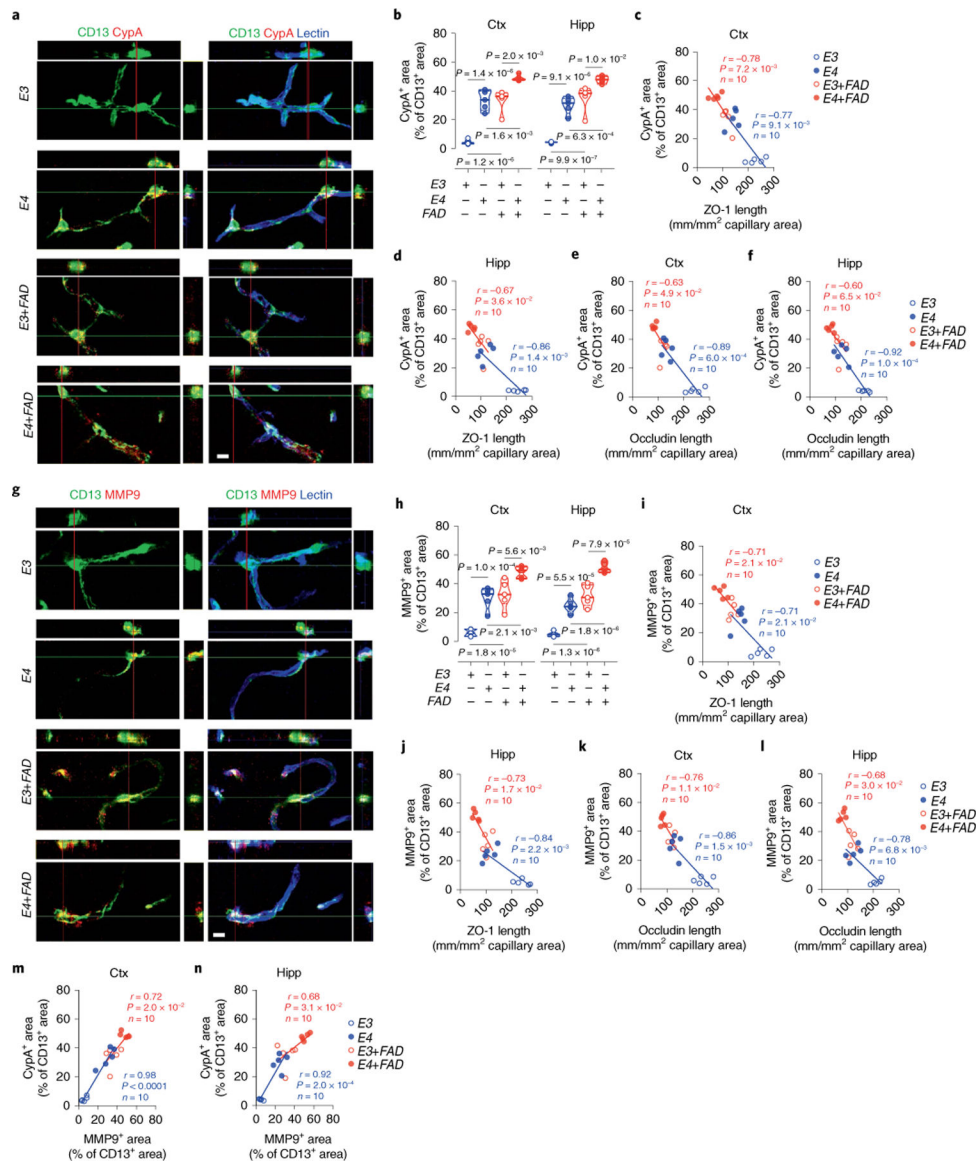
Fig. 3 |. Increased levels of cyclophilin A and matrix metalloproteinase-9 in pericytes in old *APOE4* and *APOE4;5xFAD* mice correlate with the loss of tight junction proteins.
a, Representative high-magnification confocal images of CD13+ pericytes (green), cyclophilin A (CypA; red) and lectin+ endothelium (blue) in the cortical capillaries in situ in *E3*, *E4*, *E3+FAD* and *E4+FAD* mice. Orthogonal views show colocalization of CypA with CD13+ pericytes; scale bar, 10 μm. **b**, Quantification of CypA+ pericytes in the cortex (Ctx) and hippocampus (Hipp) in *E3* (blue empty circles), *E4* (blue-filled circles), *E3+FAD* (red empty circles) and *E4+FAD* (red-filled circles) mice; *n* = 5 mice/group. **c–f**, Negative correlation between CypA+ pericytes and ZO-1 length (**c,d**), and CypA+ pericytes and occludin length (**e,f**) in the Ctx and Hipp. **g**, Representative high-magnification confocal images of CD13+ pericytes (green), MMP9 (red) and lectin+ endothelium (blue) in the cortical capillaries in situ in *E3*, *E4*, *E3+FAD* and *E4+FAD* mice. Orthogonal views show colocalization of MMP9 with CD13+ pericytes; scale bar, 10 μm. **h**, Quantification of MMP9+ pericytes in the Ctx and Hipp in *E3* (blue empty circles), *E4* (blue-filled circles),

E3+FAD (red empty circles) and *E4+FAD* (red empty circles) mice; n = 5 mice/group. **i–l**, Negative correlation between MMP9+ pericytes and ZO-1 length (**i,j**) and MMP9+ pericytes and occludin length (**k,l**) in the Ctx and Hipp. **m,n**, Positive correlation between CypA+ pericytes and MMP9 pericytes in the Ctx (**m**) and Hipp (**n**). Mice (both sexes) were 18–24 months old. Immunostaining for CypA or MMP9 and CD13, ZO-1 and lectin-endothelial staining and/or occludin and lectin-endothelial staining was performed on adjacent sections. In **b** and **h** data are presented as truncated violin plots; continuous line, median; and dotted line, interquartile range. Significance by one-way ANOVA followed by the Tukey post hoc test. In **c–f** and **i–n**, significance was obtained by by two-tailed simple linear regression. In **c–f** and **i–n**, the number was based on individual mouse values (n = 10) for *E4* versus *E3* mice in the absence of *FAD* transgenes (blue-filled and empty circles, respectively) and presence of *FAD* transgenes (red-filled and empty circles, respectively).
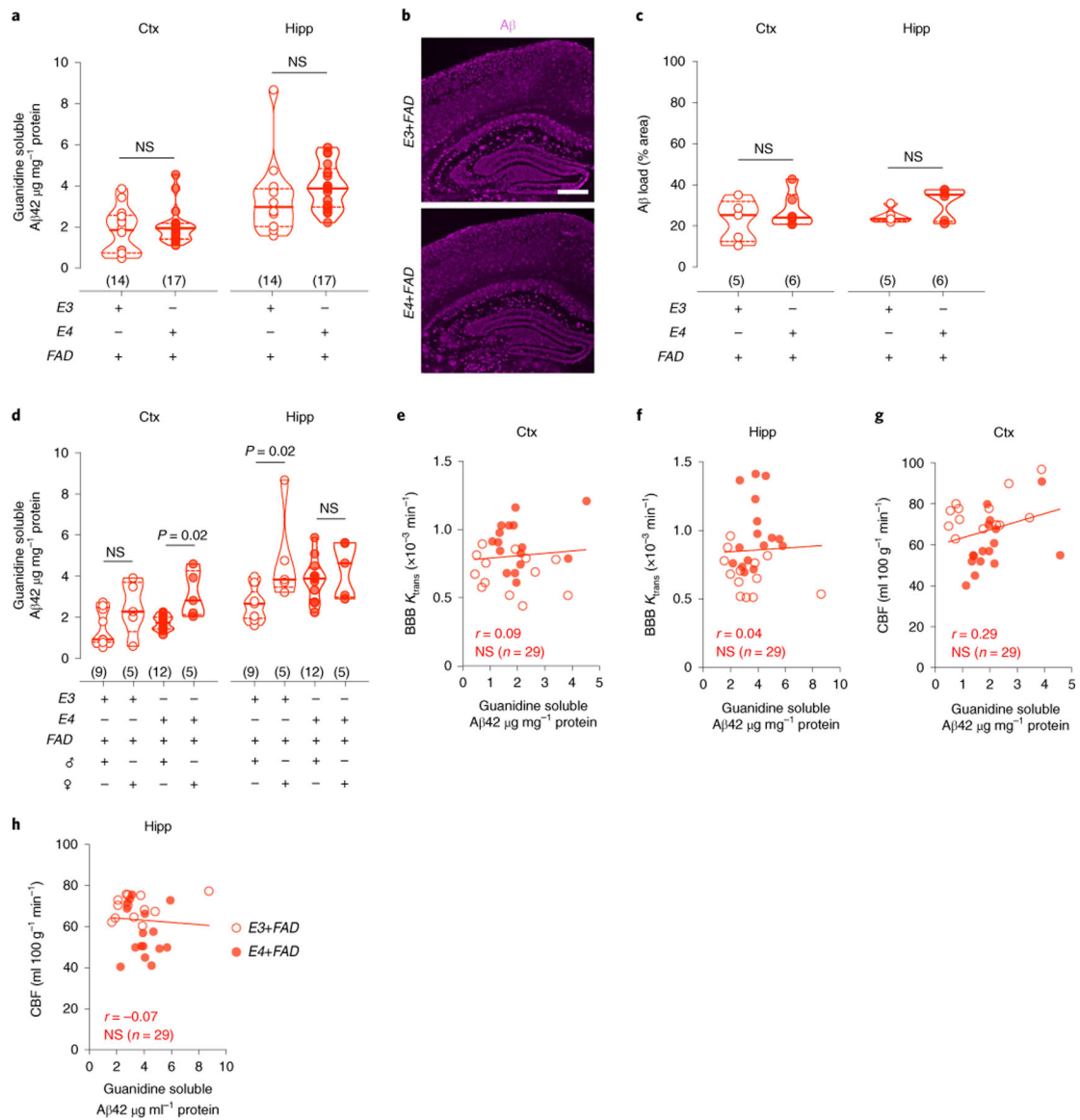
Fig. 4 |. Aβ pathology in old *APOE3*;*5xFAD* and *APOE4*;*5xFAD* mice and Aβ-independent vascular changes.

a, Aβ42 levels in the cortex (Ctx) and hippocampus (Hipp) in *E3+FAD1* (*n* = 14; red empty circles) and *E4+FAD* (*n* = 17; red-filled circles) mice. **b,c**, Aβ immunostaining (**b**) and Aβ load in the Ctx or Hipp (**c**) in *E3+FAD* (*n* = 5) and *E4+FAD* (*n* = 6) mice. Scale bar, 500 μm. **d**, Aβ42 levels in the Ctx and Hipp in male and female *E3+FAD* (*n* = 14, 9 ♂ and 5 ♀; red empty circles) and *E4+FAD* (*n* = 17, 12 ♂ and 5 ♀; red-filled circles) mice. **e–h**, Lack of correlation between the BBB permeability K_{trans} values and Aβ42 levels in the Ctx and Hipp (**e,f**) and between regional CBF values and Aβ42 levels in the Ctx and Hipp (**g,h**). Mice (both sexes) were 18–24 months old. In **d–g**, there were *n* = 29 (13 *E3+FAD* and 16 *E4+FAD*) individual mouse data points from both groups. In **a** and **c**, data are presented as violin plots; continuous line, median; and dotted line, interquartile range. Significance was obtained by unpaired two-tailed Student *t*-tests. In **d**, significance was obtained by one-way

ANOVA followed by Tukey post hoc test. In **e–h**, significance was obtained by two-tailed simple linear regression. NS, not significant.
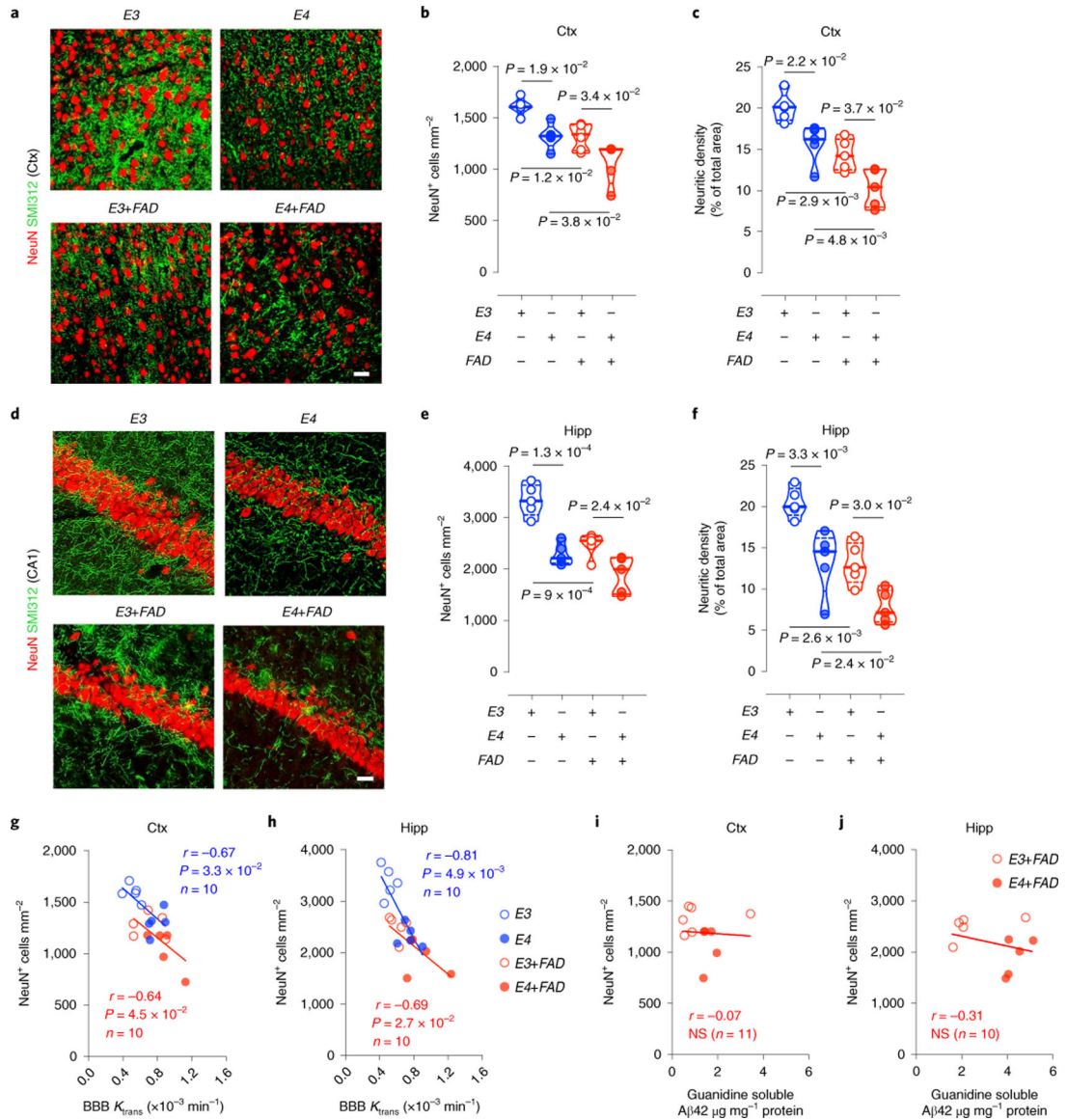
Fig. 5 |. Neurodegenerative changes in old *APOE4* and *APOE4*;*5xFAD* mice correlate with BBB breakdown but not with Aβ pathology.

a–**f**, NeuN$^+$ neurons (red) and SMI312$^+$ neurites (green) and quantification of NeuN$^+$ neurons and SMI312$^+$ neuritic density in the cortex (Ctx) (**a**–**c**) and hippocampus (Hipp) (**d**–**f**) in *E3* (*n* = 5; blue empty circles), *E4* (*n* = 5; blue-filled circles), *E3*$^+$*FAD* (*n* = 6 (**b**); *n* = 5 (**c**); n = 5 (**e**); n = 5 (**f**); red empty circles) and *E4*$^+$*FAD* (*n* = 5; red-filled circles) mice. Scale bars, 20 μm. **g**,**h**, Negative correlation between the number of NeuN$^+$ neurons and BBB permeability *K*trans values in the Ctx (**g**) and Hipp (**h**) using individual mouse data points from the studied groups. **i**,**j**, Lack of correlation between the number of NeuN$^+$ neurons and Aβ42 levels in the Ctx (**i**) and Hipp (**j**) in *E3*$^+$*FAD* (*n* = 6 (**i**); *n* = 5 (**j**)) and *E4*$^+$*FAD* (*n* = 5 (**i**); *n* = 5 (**j**)) individual mouse data points from both groups. Mice (both sexes) were 18–24 months old. In **b**,**c**,**e** and **f**, data are presented as violin plots; continuous line, median; and dotted line, interquartile range. Significance by one-way ANOVA followed

by the Tukey post hoc test. In **g**–**j**, significance was obtained by two-tailed simple linear regression. NS, not significant.

Author Manuscript

Author Manuscript

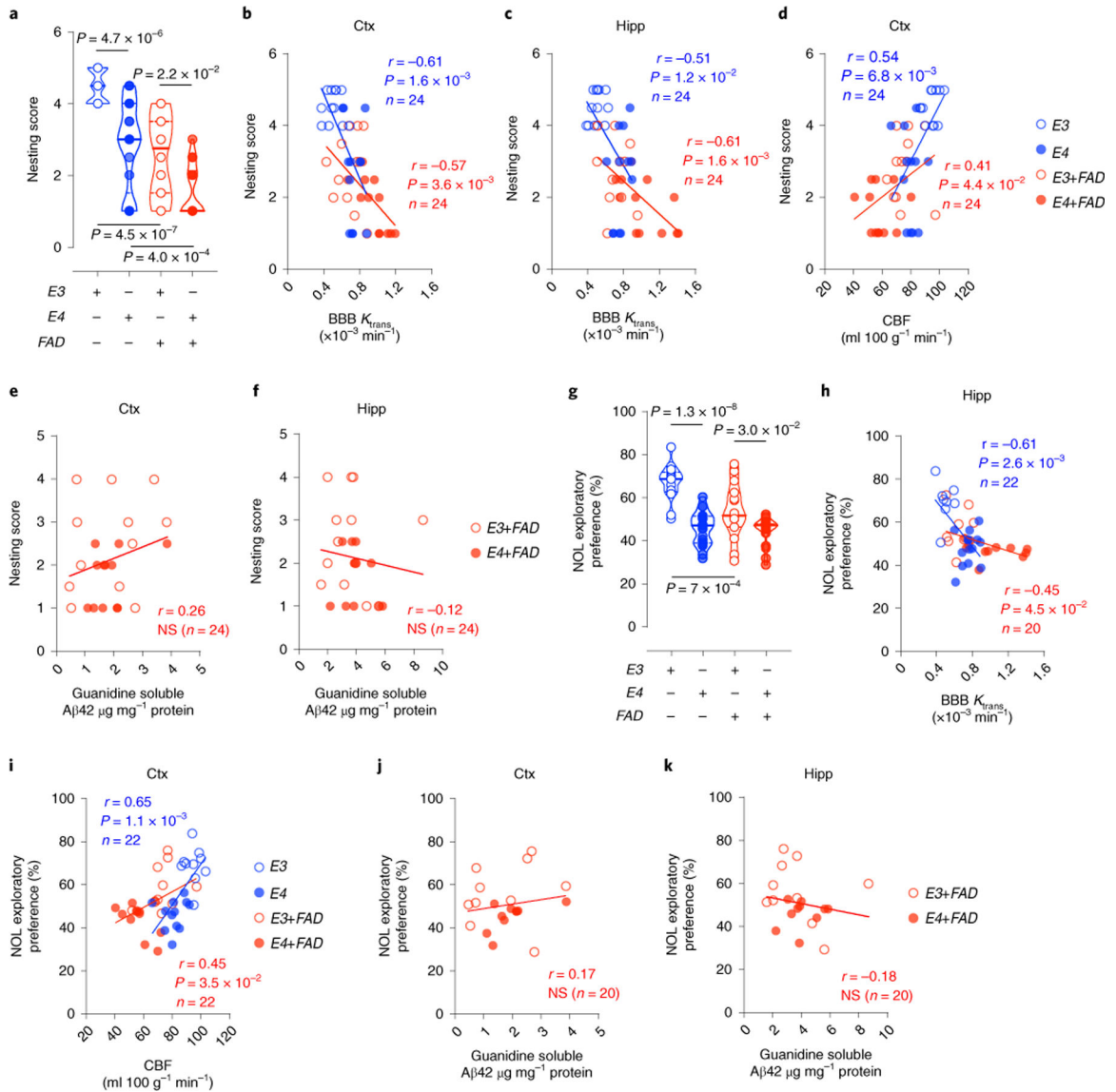Author Manuscript

Author Manuscript

Fig. 6 |. Behavioral deficits in old *APOE4* and *APOE4*;*5xFAD* mice correlate with vascular dysfunction but not with Aβ pathology.

a, Nesting scores in *E3* (*n* = 17; blue empty circles), *E4* (*n* = 25; blue-filled circles), *E3+FAD* (*n* = 18; red empty circles) and *E4+FAD* (*n* = 18; red-filled circles) mice. **b,c**, Negative correlation between nesting scores and BBB permeability K_{trans} values in the cortex (Ctx) (**b**) and hippocampus (Hipp) (**c**). **d**, Positive correlation between nesting scores and CBF values in the Ctx. In **b–d**, *n* = 48 individual mouse data points from the studied groups. **e,f**, Lack of correlation between nesting scores and Aβ42 levels in the Ctx (**e**) and Hipp (**f**); *n* = 24 individual mouse data points from the studied groups. **g**, NOL in *E3* (*n* = 15), *E4* (*n* = 21), *E3+FAD* (*n* = 15) and *E4+FAD* (*n* = 17) mice. **h**, Negative correlation between NOL and K_{trans} values in Hipp. **i**, Positive correlation between NOL and CBF values in Ctx. In **h** and **i**, *n* = 42–44 individual mouse data points from the studied groups. **j,k**, Lack of correlation between NOL values and Aβ42 levels in Ctx (**j**) and Hipp (**k**); *n* = 20 individual mouse data points from two groups. Mice (both sexes) were 18–24 months old. In **a** and

g, data are presented as violin plots; continuous line, median; and dotted line, interquartile range. Significance by one-way ANOVA followed by the Tukey post hoc test. In **b**–**f** and **h**–**k**, significance was obtained by two-tailed simple linear regression. NS, not significant.
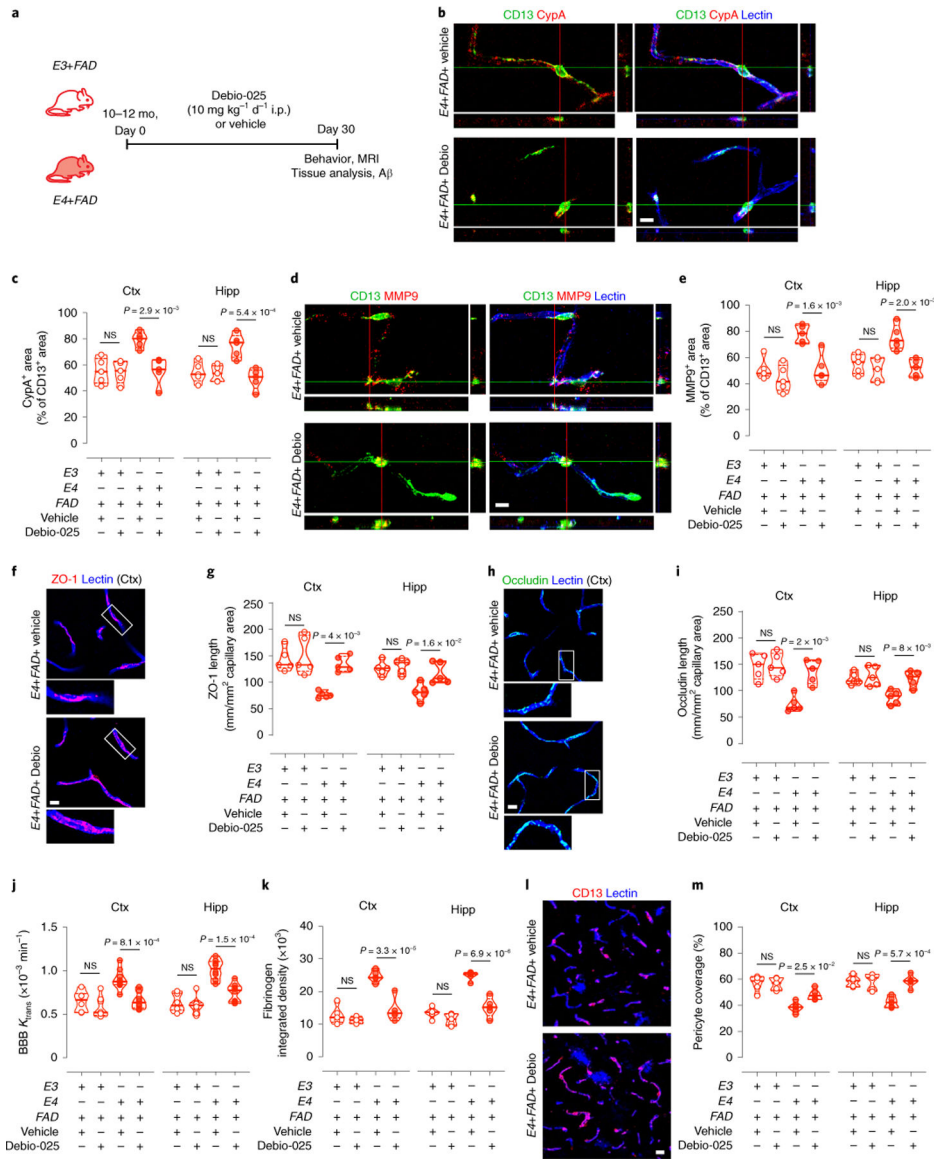
Fig. 7 |. Debio-025 inhibits the CypA-MMP9 pathway in pericytes and improves BBB integrity in *APOE4;5xFAD* mice.

a, A schematic of the time course of Debio-025 experiment. **b**, Confocal images of CD13^{+} pericytes (green), CypA (red) and lectin^{+} endothelium (blue) in the cortical capillaries in *E4^{+}FAD* mice treated with vehicle or Debio-025. Orthogonal views, colocalization of CypA with CD13^{+} pericytes; scale bar, 10 μm. **c**, Quantification of CypA^{+} pericytes in the cortex (Ctx) and hippocampus (Hipp) in *E3^{+}FAD* (red empty circles) and *E4^{+}FAD* (red-filled circles) mice treated with vehicle or Debio-025; *n* = 5 mice per group. d, Confocal images of CD13^{+} pericytes (green), MMP9 (red) and lectin^{+} endothelium (blue) in cortical capillaries in *E4^{+}FAD* mice treated with vehicle or Debio-025. Orthogonal views, colocalization of MMP9 with CD13^{+} pericytes; scale bar, 10 μm. **e**, Quantification of MMP9^{+} pericytes in the Ctx and Hipp in *E3^{+}FAD* (red empty circles) and *E4^{+}FAD* (red-filled circles) mice treated with vehicle or Debio-025; *n* = 5 mice per group. **f,g** Immunostaining for ZO-1 (red) and lectin[+] endothelium (blue) in the Ctx in *E4[+]FAD* mice treated with vehicle or Debio-025 (**f**,

red) and ZO-1 length in the Ctx and Hipp (**g**) in *E3⁺FAD* (red empty circles) and *E4⁺FAD* (red-filled circles) mice treated with vehicle or Debio-025; $n = 5$ mice per group; scale bar, 20 μm. **h–i**, Immunostaining for occludin (green) and lectin⁺ endothelium (blue) in the Ctx (**h**, green) and occludin length in the Ctx and Hipp (**i**) in *E3⁺FAD* (red empty circles) and *E4⁺FAD* (red-filled circles) mice treated with vehicle or Debio-025; $n = 5$ mice per group; scale bar, 20 μm. Boxes in **f** and **h** denote sites taken for higher magnification insets shown below merged images. **j**, BBB permeability K_{trans} values in the Ctx and Hipp in *E3⁺FAD* vehicle-treated ($n = 6$; red empty circles), *E3⁺FAD* Debio-025-treated ($n = 8$; red empty circles), *E4⁺FAD* vehicle-treated ($n = 8$; red-filled circles) and *E4⁺FAD* Debio-025-treated ($n = 8$; red-filled circles) mice. **k**, Quantification of fibrinogen⁺ pericapillary deposits in the Ctx and Hipp in *E3⁺FAD* (red empty circles) and *E4⁺FAD* (red-filled circles) mice treated with vehicle or Debio-025; $n = 5$ mice per group. **l,m**, CD13⁺ pericyte coverage (magenta) of lectin⁺ endothelial capillary profiles (blue) in the Ctx (**l**; scale bar, 20 μm) and quantification of pericyte capillary coverage in the Ctx and Hipp (**m**) in *E3⁺FAD* (red empty circles) and *E4⁺FAD* (red-filled circles) mice treated with vehicle or Debio-025; $n = 5$ mice per group (scale bar, 20 μm). Mice (both sexes) were 10–12 months old. In **c,e,g,i–k** and **m** data are presented as truncated violin plots; continuous line, median; and dotted line, interquartile range. Significance was determined by one-way ANOVA followed by the Tukey post hoc test.
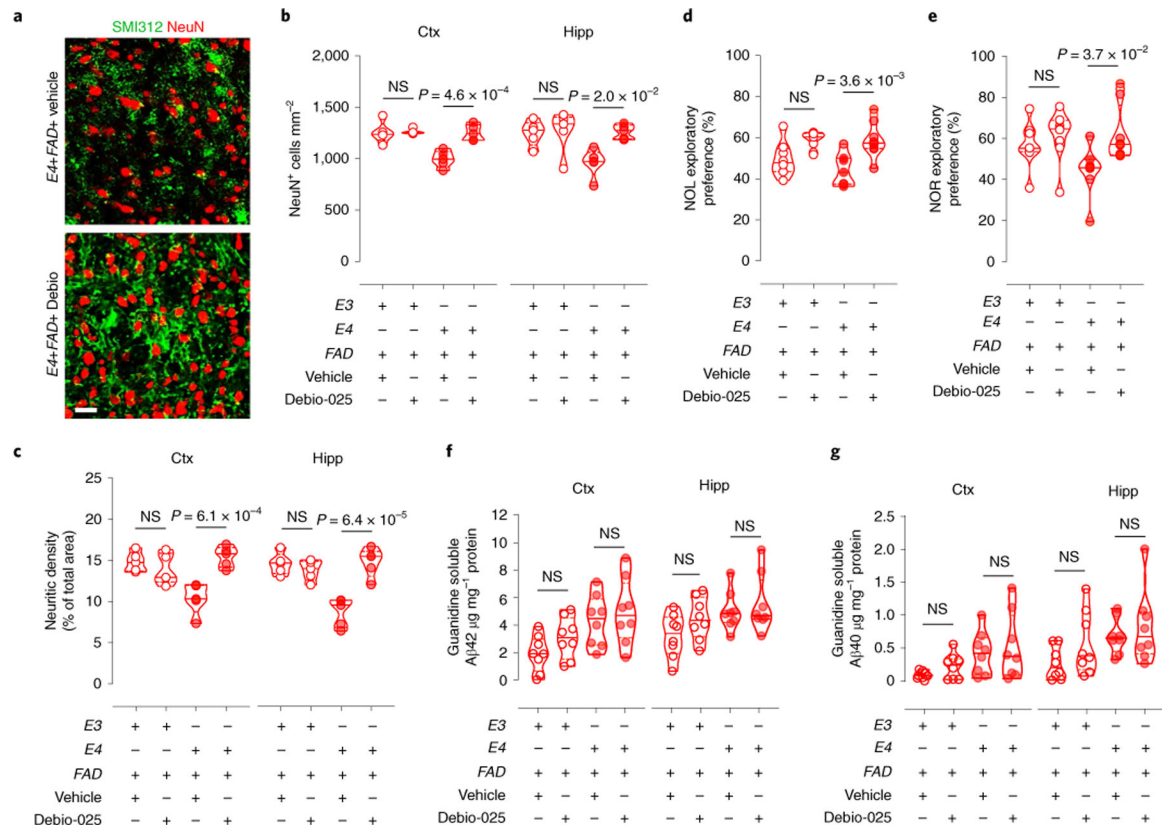
Fig. 8 |. Debio-025 prevents further loss of neurons and improves cognitive function in
***APOE4;5xFAD* mice without affecting Aβ42 or Aβ40 levels in the brain.**
a–**c**, Cortical NeuN+ neurons (red) and SMI312+ neurites (green) (**a**) and quantification of
NeuN+ neurons (**b**) and SMI312+-neuritic density (**c**) in the cortex (Ctx) and hippocampus
(Hipp) in *E3+FAD* (red empty circles) and *E4+FAD* (red-filled circles) mice treated with
vehicle or Debio-025; *n* = 5 mice per group. Scale bar, 20 μm. **d,e**, NOL (**d**) and NOR (**e**)
in *E3+FAD* vehicle-treated (*n* = 8; red empty circles), *E3+FAD* Debio-025-treated (*n* = 9; red
empty circles), *E4+FAD* vehicle-treated (*n* = 7; red-filled circles) and *E4+FAD* Debio-025-
treated (*n* = 8; red-filled circles) mice. **f,g**, Aβ42 (**f**) and Aβ40 (**g**) levels in the Ctx and
Hipp in *E3+FAD* vehicle-treated (*n* = 8; red empty circles), *E3+FAD* Debio-025-treated (*n*
= 8; red empty circles), *E4+FAD* vehicle-treated (*n* = 8; red-filled circles) and *E4+FAD*
Debio-025-treated (*n* = 8; red-filled circles) mice. Mice (both sexes) at 10–12 months old
were the same as in Fig. 7. In **b**–**g**, data are presented as violin plots; continuous line,
median; and dotted line, interquartile range. Significance was obtained by one-way ANOVA
followed by Tukey post hoc test.